Biosci. Rep. (2012) / **32** / 401–411 (Printed in Great Britain) / doi 10.1042/BSR20120037

online data

Original Paper

Allosteric modulation of caspase 3 through mutagenesis

Jad WALTERS*, Joshua L. SCHIPPER*, Paul SWARTZ*, Carla MATTOS*[1] and A. Clay CLARK*†[2]

*Department of Molecular and Structural Biochemistry, North Carolina State University, Raleigh, NC 27695, U.S.A., and †Center for Comparative Medicine and Translational Research, North Carolina State University, Raleigh, NC 27695, U.S.A.

Synopsis

A mutation in the allosteric site of the caspase 3 dimer interface of Val^{266} to histidine abolishes activity of the enzyme, and models predict that the mutation mimics the action of small molecule allosteric inhibitors by preventing formation of the active site. Mutations were coupled to His^{266} at two sites in the interface, E124A and Y197C. We present results from X-ray crystallography, enzymatic activity and molecular dynamics simulations for seven proteins, consisting of single, double and triple mutants. The results demonstrate that considering allosteric inhibition of caspase 3 as a shift between discrete 'off-state' or 'on-state' conformations is insufficient. Although His^{266} is accommodated in the interface, the structural defects are propagated to the active site through a helix on the protein surface. A more comprehensive view of allosteric regulation of caspase 3 requires the representation of an ensemble of inactive states and shows that subtle structural changes lead to the population of the inactive ensemble.

Key words: allosteric site, apoptosis, caspase, inhibition, protein ensemble.

Cite this article as: Walters, J., Schipper, J.L., Swartz, P. Mattos, C. and Clark, A.C. (2012) Allosteric modulation of caspase 3 through mutagenesis. Biosci. Rep. **32**, 401–411

INTRODUCTION

A common allosteric mechanism for caspase inhibition involves short-range interactions between amino acids in the dimer interface and active site residues [1]. Disrupting the interactions, either through mutagenesis [2,3] or through the binding of small molecules [4] destabilizes the active conformation and shifts the protein into the inactive or 'closed' state. Procaspase 3 is a stable but inactive homodimer, where the 'monomer' consists of a large and small subunit covalently connected by a linker of 17 amino acids. Upon cleavage of the IL (intersubunit linker) by initiator caspases, the polypeptide chain is released from its binding in the dimer interface cavity, allowing the substrate-binding loop (called L3) to move into the active site and form the base of the substrate-binding pocket [5]. Loop movement leading to activation of cleaved caspases has been reviewed recently, and the reader is referred to the references therein [6]. As a consequence of IL cleavage, Arg^{164}, which resides adjacent to the catalytic Cys^{163}, moves from a solvent-exposed position in the procaspase to a buried position in the dimer interface of the mature caspase, where it intercalates between Tyr^{197} and Pro^{201}. The binding of inhibitors in the allosteric site of the interface reverses the conformational change by preventing insertion into the interface of a region of L3 known as the 'elbow loop', which contains Pro^{201} [1,7]. The stacking interactions between Tyr^{197}, Arg^{164} and Pro^{201} are thought to stabilize the active conformation.

We showed that the allosteric site in the dimer interface is bifunctional and depends on the context of the protein. The same site that inactivates the mature caspase also can activate the procaspase [2,6]. For example, a mutation of Val^{266} to glutamate in the dimer interface results in a constitutively active procaspase 3. The procaspase is activated without chain cleavage because the mutation shifts the conformational ensemble to an active state. The constitutively active procaspase 3 rapidly kills cells, and importantly, the protein is inhibited poorly by XIAP (X-linked inhibitor of apoptosis), the endogenous caspase 3 inhibitor [8]. A model of the activated procaspase 3 suggests that the mutation prevents binding of the IL in the dimer interface, essentially destabilizing the inactive conformer and favouring the active conformer [8]. In a broader context, the results imply that introducing the activated procaspase 3 in a targeted manner may be an effective method for killing specific cells. Alternatively, small molecules also activate procaspase 3 allosterically through

Abbreviations used: DTT, dithiothreitol; IL, intersubunit linker; RMSD, root mean square deviation.

[1] Present address: Department of Chemistry and Chemical Biology, Northeastern University, 102 Hurtig Hall, 360 Huntington Ave, Boston, MA 02115, U.S.A.

[2] To whom correspondence should be addressed (email clay_clark@ncsu.edu).

binding to the dimer interface [6] or other sites [4], presumably by a similar mechanism of releasing the IL from the interface.

Collectively, current results suggest that the ensemble of conformations is more complex than a simple two-state model, where the IL of the inactive procaspase 3 is cleaved by initiator caspases to yield the fully active mature caspase. Indeed, it has long been known that, in the absence of substrate, mature caspase 7 exists in the closed conformation. In this case, the cleaved IL remains bound in the dimer interface, and the protein rearranges to the active conformer in the presence of substrate [9,10].

In contrast with the V266E mutant of caspase 3, a mutation of Val^{266} to histidine was shown to inactivate the protein [2], and it was suggested that steric clashes in the interface prevent insertion of the elbow loop and Arg^{164}, essentially mimicking the mechanism of the small molecule allosteric inhibitors [2,11]. In order to more fully understand the allosteric site of the caspase 3 dimer interface and the effect that amino acid mutations in the interface have on allosteric regulation, we determined the structure of the V266H variant by X-ray crystallography, and the results pointed to several residues that could potentially be involved in the mechanism of allosteric inhibition. We subsequently mutated those residues in the background of V266H and report the X-ray crystal structures of those proteins as well. Overall, results from crystallography, enzymology and molecular dynamics simulations show that allosteric regulation is more complex than a single short-range interaction pathway involving Arg^{164}. The results demonstrate long-range connectivity between the interface allosteric site and the active site loops. The results also show that the conformational ensemble of inactive versus active states can be influenced by the interactions of several key residues, some of which are buried in the interface while others reside on the protein surface. Allosteric manipulation of the (pro)caspase conformational ensembles may provide new therapeutic interventions for either promoting or preventing apoptosis, but currently the ensembles are poorly understood.

MATERIALS AND METHODS

Cloning, expression and purification

Mutagenesis of caspase 3 to generate the single, double and triple mutants was performed as described in the Supplementary information available online at http://www.bioscirep.org/bsr/032/bsr0320401add.htm. *Escherichia coli* BL21(DE3) pLysS cells were transformed with each of the plasmids, and all proteins were expressed and purified following previously established protocols [2,12–14]. Caspase 3 (V266H) and caspase 3 (E124A and V266H) are enzymatically inactive (described below), and the protein purified as the procaspase form. The cleaved form was generated by treating with granzyme B (Calbiochem) in a buffer of 20 mM Hepes, 100 mM NaCl, 0.1 % CHAPS, 10 % sucrose and 10 mM DTT (dithiothreitol) (enzyme assay buffer) at 37 °C for 2 h at a final caspase/granzyme B molar ratio of 90:1.

Crystallization and data collection

Proteins were dialysed in a buffer of 10 mM Tris/HCl, pH 8.5, and 1 mM DTT and concentrated to 10 mg/ml. Inhibitor, Ac-DEVD-CMK (acetyl-Asp-Glu-Val-Asp-chloromethyl ketone) reconstituted in DMSO, was then added at a 5:1 (w/w) inhibitor/peptide ratio. The protein was diluted to a concentration of 8 mg/ml by adding 10 mM Tris/HCl, pH 8.5, concentrated DTT, and concentrated NaN_3 so that the final buffer consisted of 10 mM Tris/HCl, pH 8.5, 10 mM DTT and 3 mM NaN_3. Crystals were obtained at 18 °C by the hanging drop vapour diffusion method using 4 μl drops that contained equal volumes of protein and reservoir solutions over a 0.5 ml reservoir. The reservoir solutions for optimal crystal growth consisted of 100 mM sodium citrate, pH 5.0, 3 mM NaN_3, 10 mM DTT and $10-16$ % (w/v) PEG [poly(ethylene glycol)] 6000. Crystals appeared within 3.5–6 weeks for all mutants and were briefly immersed in cryogenic solution containing 10 % MPD (2-methylpentane-2,4-diol) and 90 % reservoir solution. Data sets were collected at 100 K at the SER-CAT synchrotron beamline (Advance Photon Source, Argonne National Laboratory, Argonne, IL, U.S.A.) The X-rays had a wavelength of 1 Å (where 1 Å = 0.1 nm), and 180° of data were collected for each protein at 1° intervals. Those mutants that crystallized with the symmetry of the orthorhombic space group I222 were phased with a previously published caspase 3 structure (PDB entry 2J30), as described [8]. Caspase 3 mutants that crystallized with the symmetry of the monoclinic space group C2 were phased with another previously published structure (PDB entry 1NMS). A summary of the data collection and refinement statistics is shown in Supplementary Table S1 (at http://www.bioscirep.org/bsr/032/bsr0320401add.htm). The atomic co-ordinates and structure factors for caspase 3 (V266H), caspase 3 (Y197C), caspase 3 (E124A), caspase 3 (Y197C,V266H), caspase 3 (E124A,Y197C) caspase 3 (E124A,V266H) and caspase 3 (E124A,Y197C,V266H) have been deposited in the PDB under accession codes 4EHA, 4EHD, 4EHH, 4EHF, 4EHK, 4EHL and 4EHN respectively.

Enzyme activity assay

Initial velocity was measured in enzyme assay buffer at 25 °C in the presence of varying concentrations of Ac-DEVD-AFC (acetyl-Asp-Glu-Val-Asp-7-amino-4-trifluoromethylcoumarin) substrate, as described previously [2,14–16]. The total reaction volume was 200 μl and the final enzyme concentration was 10 nM. Briefly, following addition of the substrate, the samples were $\lambda_{excitation}$ at 400 nm, and $\lambda_{emission}$ was monitored at 505 nm for 60 s. The steady-state parameters, K_m and k_{cat}, were determined from plots of initial velocity versus substrate concentration.

Molecular dynamics simulations

Molecular dynamics simulations were performed with GROMACS 4.5 [17], using the Amber99 force field [18] and the TIP3P water model [19]. All simulations started with structures obtained from X-ray crystallography as described above.

For those proteins that crystallized with symmetry of the space group I222, with one monomer in the asymmetric unit, as was the case for wild-type caspase 3, dimers were generated by applying the appropriate 2-fold crystallographic symmetry. The proteins were solvated in a periodic box of 62 Å × 48 Å × 66 Å, with approximately 13 500 water molecules. Sodium or chloride ions were added as required to neutralize the charge on the system. The system was first minimized using steepest descent, and then the waters were relaxed during a 20 ps MD simulation with positional restraints on the protein. Simulations of 50 ns were then run for each protein under constant pressure and temperature (300 K). A time step of 2 fs was used, and co-ordinates were saved every 5 ps. A cut-off radius of 9 Å was used for non-bonded interactions, and electrostatic interactions were calculated using the Particle Mesh Ewald method [20]. In each simulation, the protein was equilibrated within 500 ps. Cavity volumes were estimated by multiplying the number of water molecules within 15 Å of the α carbon atom of residue 266 by the average volume of a single water molecule ($\sim$17 Å^3), which was consistent throughout each simulation.

RESULTS

X-ray crystal structure of caspase 3 (V266H) reveals long-range interactions

In wild-type caspase 3, van der Waals interactions between Val^{266} and Tyr^{197} from each monomer provide close packing in the dimer interface. Our initial model of caspase 3 (V266H) [11] explained inhibition by a steric hindrance model, assuming that the His^{266}–His$^{266'}$ residues were in the preferred rotamer for histidine in which the side chains face each other edge-on across the interface (the prime ($'$) refers to residues in the second monomer). In this model, the ε_2-nitrogen atom of each histidine ring faces Arg^{164}, but the ring also partially occupies the space for Tyr^{197}. It was thought that steric clashes between the His^{266} and Tyr^{197} side chains would prevent proper insertion of Arg^{164} into the dimer interface, thus destabilizing the active site. A very similar case is seen in caspase 9, where the presence of several bulky residues in the interface prohibits the formation of two productive active sites [21], so one active site forms, while the other remains disordered. Although the steric-hindrance model was feasible based on our current understanding of the caspase 3 allosteric site, the structure of caspase 3 (V266H) showed a very different story.

Wild-type caspase 3 crystallizes with the symmetry of the orthorhombic space group I222, containing one monomer per asymmetric unit, so the biological dimer of caspase 3 is generated through one of the two-fold crystallographic symmetry axis. Caspase 3 (V266H), however, crystallized with the symmetry of the monoclinic space group C2, which contains two monomers per asymmetric unit. From this information alone one can infer that the monomers are no longer symmetric in the V266H variant, and examination of the structure showed this to be true. The backbone atoms of both monomers superimpose reasonably well with the monomer of wild-type caspase 3 [RMSD (root mean square deviation) $\sim$0.17 Å], but the dimer demonstrates a larger difference (RMSD = 0.34 Å) because of differences in active site loop 1 and amino acid side chains in the interface of monomer B, so the description presented here focuses on monomer B. Surprisingly, the variant is able to accommodate the bulky histidine residues due to a 90° rotation about φ_2 so that the histidine rings face each other across the interface (Figure 1A; see also Supplementary Figure 3B available online at http://www.bioscirep.org/bsr/032/bsr0320401add.htm). One observes several changes in the interface of the mutant when compared with that of wild-type caspase 3. The hydroxy group of Tyr^{197} is displaced $\sim$0.8 Å away from the interface, and the movement is accompanied by an even larger shift in Tyr^{195}, where the hydroxy group moves $\sim$2.3 Å away from the interface (Figure 1A). In contrast, small changes are observed for the short-range allosteric residues Arg^{164} and Pro^{201}, although we note that the proline residue contains a different ring pucker compared with that of wild-type. In addition, there are minor changes for Glu^{124}, which resides above the interface and neutralizes the charge of Arg^{164}. Overall, the structure of the V266H variant demonstrated that the inhibition could not be explained by disruption of the short-range allosteric network because the His^{266}–His$^{266'}$ side chains were accommodated in the interface, albeit with repositioning of neighbouring tyrosine side chains.

Expanding away from the site of the mutation, one observes the consequences of the movements in the side chains of Tyr^{197} and Tyr^{195}. In wild-type caspase 3, Tyr^{195} participates in a H-bonding network with Lys^{137}, Thr^{140}, Glu^{190} and two water molecules. The hydroxy group of Tyr^{195} forms through-water H-bonds with Glu^{190} and Thr^{140} (Figure 1B, upper panel). The Glu^{190} residue has been shown previously to be important for stabilizing the active site because it forms backbone H-bonds with Asp$^{169'}$ across the interface and stabilizes active site loops 2 and 2$'$ downstream of the catalytic Cys^{163} in the so-called 'loop bundle.' (Figure 1C) [13,22]. In the V266H variant, by contrast, the Tyr^{195} hydroxy group moves to within 2.9 Å of the side chain of Thr^{140} and forms a direct H-bond (Figure 1B, lower panel, and Supplementary Figures S1A and S1B at http://www.bioscirep.org/bsr/032/bsr0320401add.htm). Although one water molecule in the Tyr^{195}–Glu^{190} H-bond network is conserved in the mutant, a second water molecule replaces the hydroxy group from wild-type Tyr^{195} so that the interaction with Glu^{190} now occurs through two waters. In addition, a salt bridge observed in wild-type caspase 3 between Lys^{137} and Glu^{190} (Figure 1B, upper panel) is disrupted in the V266H mutant (Figure 1B, lower panel, and Supplementary Figures S1A and S1B). Although the side chain of Glu^{190} appears to be unaffected by the movement in Tyr^{195} and the loss of the salt bridge with Lys^{137}, the structural data suggest that the conformational changes may be propagated across the dimer interface to affect the opposing active site by destabilizing the L2–L2$'$ loop bundle. The dynamics of this region are addressed more fully below.

The side chain of Thr^{140} is positioned near the water-filled interface cavity in the middle of helix 3, one of five surface helices (Figure 1C). In the mutant, the direct H-bond between Tyr^{195} and

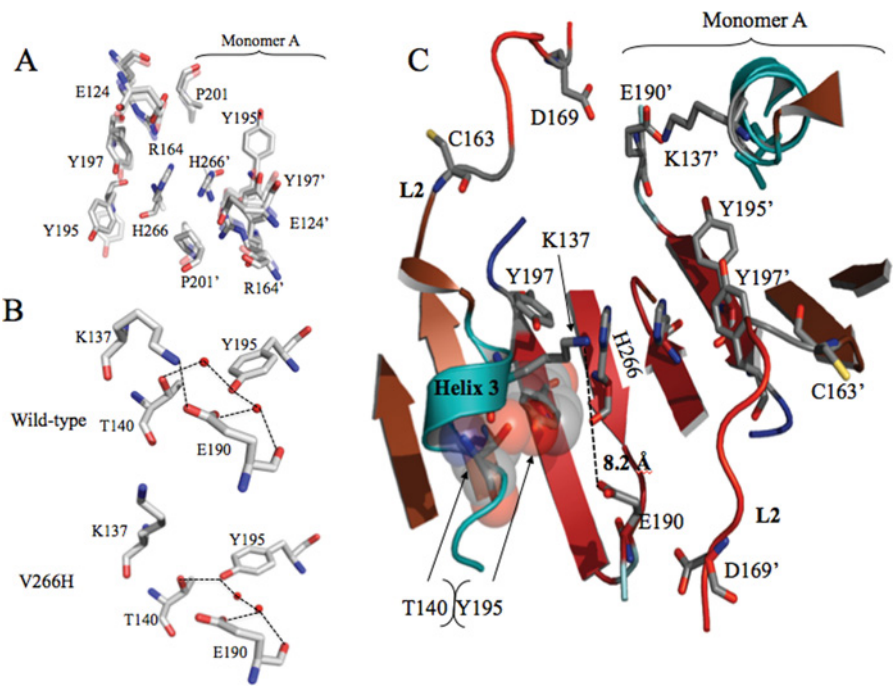

Figure 1 **Amino acids in the dimer interface of caspase 3**
(**A**) Interface of caspase 3 (V266H) determined by X-ray crystallography (solid) overlaid with that of wild-type caspase 3 (transparent). (**B**) Interactions among Lys[137], Thr[140], Glu[190] and Tyr[195] in wild-type (upper panel) or V266H (lower panel) caspase 3. The red spheres indicate water molecules. (**C**) Broader view of residues from (**B**) in caspase 3 (V266H) demonstrating increased distance between Lys[137] and Glu[190] as well as interactions across the dimer interface.

Thr[140] distorts the N-terminus of helix 3 such that it moves by ~1 Å (Figure 2A), which may be the cause of the repositioning of Lys[137]. The movements are propagated further through two short β-strands on the protein surface, again by ~1–2 Å, so that the protein chain moves closer to the active site. Ultimately, Phe[128], on one of the surface β-strands, clashes with Met[61] (on active site L1). The movement results in a different rotamer for Met[61] such that the side chain moves towards His[121], the second catalytic residue, and affects its H-bonding with Thr[62] in active site L1 (Figure 2A and Supplementary Figures S1C and S1D). The S1 binding pocket is narrower in the mutant because of partial occupation by the His[121] side chain (Supplementary Figure S2 at http://www.bioscirep.org/bsr/032/bsr0320401add.htm). Overall, the structural data show that the mutation in the dimer interface at His[266] is propagated through helix 3 to the surface of the protein in a way that results in a disordered L1 (Figures 2B and 2C) and a narrower S1-binding pocket.

Mutations coupled to V266H restore the enzyme activity

In order to further examine the changes in the dimer interface that result from the V266H mutation, we replaced Tyr[197] with cysteine and Glu[124] with alanine, both singly and in combination with the V266H mutation (Figure 3A). As noted above, Glu[124] resides on a loop above the dimer interface, where the loop connects the two short β-strands that were observed to move in the V266H mutant. The side chain of Glu[124] also neutralizes the positive charge of Arg[164] (see Figure 1), so, in addition to the stacking interactions with Tyr[197] and Pro[201], the three residues (Glu[124], Tyr[197] and Pro[201]) are thought to stabilize Arg[164] in the active conformation.

Both single mutants, Y197C and E124A, exhibited about 3–4-fold lower activity than wild-type caspase 3 (Table 1 and Figure 3A), which was manifested primarily in lower k_{cat} values and a $\Delta\Delta G^{\circ}$ of ~0.6–1 kcal/mol. When combined, however, the double mutant, E124A,Y197C, had an ~100-fold lower activity, with an additional $\Delta\Delta G^{\circ}$~1.8–2.2 kcal/mol. The results indicated that while either single mutant was reasonably well tolerated, loss of both residues dramatically decreased activity.

When placed in context of the His[266] variant, E124A had no effect on activity, that is, the E124A and V266H double mutant remained inactive. In contrast, the mutation of Tyr[197] to cysteine in the context of V266H resulted in an increase in activity such that the activity of Y197C,V266H was only ~15-fold lower than that of wild-type caspase 3. There was no further increase in activity in the triple mutant compared with Y197C,V266H [~$(0.9–1.7)\times10^{3}$ $M^{-1}\cdot s^{-1}$], although it is notable that the activity of the triple mutant is greater than that of the E124A,Y197C double mutant by approximately 3-fold.

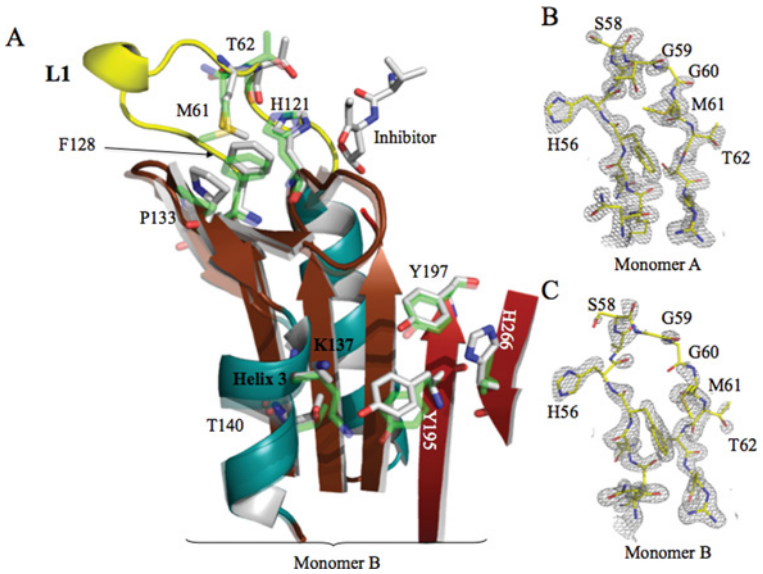

Figure 2 **Comparison of changes resulting from the Val^{266} to histidine mutation**
(**A**) Conformational changes in the dimer interface, helix 3 and active site of the V266H variant compared with wild-type caspase 3. The wild-type protein is shown as partially transparent secondary structure with amino acid side chains in green. The electron density maps of loop 1 from monomer A (**B**) or monomer B (**C**) show disorder in L1 of monomer B.

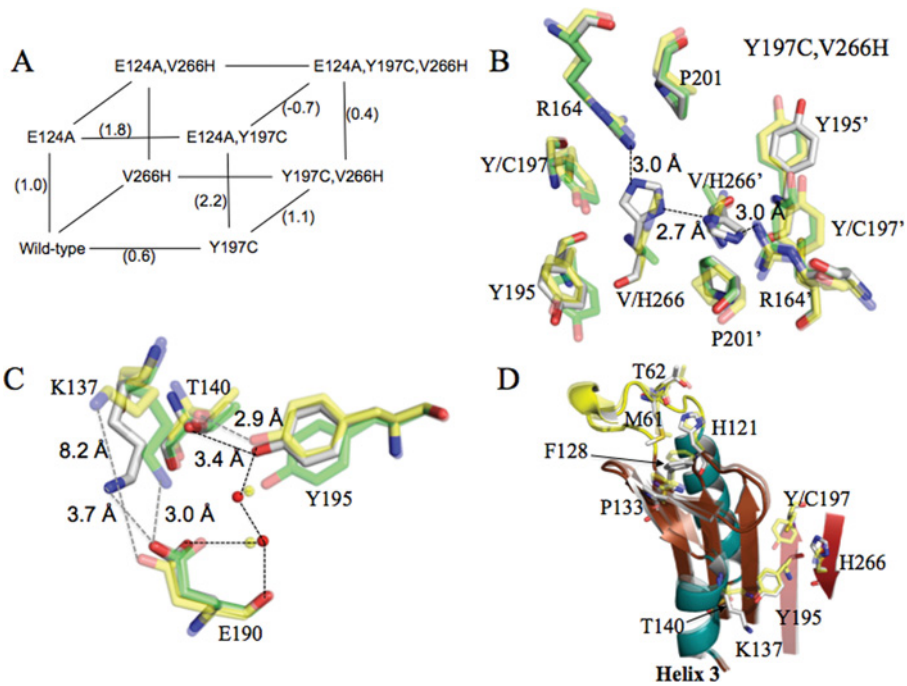

Figure 3 **A double mutation of Y197C,V266H restores activity and structure similar to that of wild-type**
(**A**) Additional mutations made in the context of V266H. Numbers in parentheses indicate change in k_{cat}/K_m values in terms of $\Delta\Delta G^{\circ}$ (kcal/mol), as described in the text. (**B**) Dimer interface of caspase-3 (Y197C,V266H). (**C**) Interactions among Lys^{137}, Thr^{140}, Glu^{190} and Tyr^{195}. (**D**) Comparison of changes in helix 3 and the active site of monomer B. For (**B–D**), the following colour scheme is used: Y197C,V266H (grey), V266H (yellow) and wild-type (green).

Table 1 Catalytic parameters of the caspase 3 interface mutants
N.D., no measurable activity.

Protein	K_m (μM)	k_{cat} (s^{-1})	k_{cat}/K_m ($M^{-1} \cdot s^{-1}$)
Wild-type*	14 ± 6	0.4 ± 0.05	2.86×10^4
V266H†	>50	N.D.	N.D.
Y197C	9.5 ± 1	0.10 ± 0.01	1.05×10^4
E124A	27 ± 4	0.14 ± 0.01	5.19×10^3
Y197C,V266H	12 ± 4	$0.02 \pm (2 \times 10^{-3})$	1.67×10^3
E124A,V266H	>50	N.D	N.D.
E124A,Y197C	30 ± 5	$0.008 \pm (3 \times 10^{-4})$	2.67×10^2
E124A,Y197C, V266H	22 ± 3	$0.02 \pm (1 \times 10^{-3})$	9.10×10^2

*From Feeney et al. [13].
†From Pop et al. [2].

X-ray crystal structures of variants coupled to V266H

The structures of the proteins shown in Figure 3(A) were determined by X-ray crystallography to resolutions >1.86 Å (Supplementary Table S1). Both single mutants, Y197C and E124A, crystallized in the orthorhombic space group I222, the same as wild-type caspase 3. The monomer of both proteins superimposed well with that of wild-type, with RMSD of 0.122 and 0.127 Å respectively. When the interfaces are compared with that of wild-type, one observes minor changes at the site of the mutation. The interface allosteric site of wild-type caspase 3 contains six conserved water molecules that form H-bonds across the dimer interface between Arg^{164}, Tyr^{197}, $Arg^{164'}$, and $Tyr^{197'}$ [8] (Supplementary Figure S3A at http://www.bioscirep.org/bsr/032/bsr0320401add.htm). The six water molecules also are retained in the two mutants (Supplementary Figures S3C and S3D) as is the extensive H-bonding network in the interface. In the E124A variant, however, the side chain of Tyr^{195} is shifted 1.1 Å away from the interface so that it is 3.6 Å from Thr^{140} (Supplementary Figure S3D). In a broader view, there are no differences in helix 3, the two surface β-strands, or the active sites when compared with wild-type caspase 3 (Supplementary Figure S5 at http://www.bioscirep.org/bsr/032/bsr0320401add.htm).

The double mutant, E124A,V266H, crystallized in the monoclinic space group C2, the same as the single mutant V266H. Overall, the structure is very similar to caspase 3 (V266H), with movements along the protein surface between the interface and loop 1 (Supplementary Figure S6 at http://www.bioscirep.org/bsr/032/bsr0320401add.htm). The hydroxy group of Tyr^{195} is in a similar position as it is in the V266H variant, ~3 Å from Thr^{140}, although the side chain of Lys^{137} is similar to that of wild-type and interacts with Glu^{190} (Supplementary Figure S6B). Surprisingly, the electron density supports two conformations for His^{266} in monomer B, where one conformation is similar to that observed in the V266H single mutant (Figure 1A) and the second conformation faces Tyr^{195} (Supplementary Figures S6A and S6C). In monomer A, the electron density supports only one conformation for His^{266}, similar to that in the V266H variant.

The double mutant, E124A,Y197C, also crystallized in the monoclinic space group C2. As described above, this mutant demonstrated very low enzymatic activity, and the structure showed several features in common with the V266H variant (Supplementary Figures S7A and S7B at http://www.bioscirep.org/bsr/032/bsr0320401add.htm). When compared with wild-type caspase 3, the overall RMSD is 0.23 Å, and the side chain of Tyr^{195} is positioned ~3.2 Å from that of Thr^{140}. Helix 3 is somewhat distorted, and the surface β-strands are moved towards the interface, with surface side chains nearly identical with those of the V266H variant and loop 1 partially disordered (Supplementary Figure S7C). In contrast with the V266H variant, however, the side chain of Met^{61} is similar to that of wild-type caspase 3, and the side chain of Lys^{137} also is positioned similarly to that of wild-type and interacts directly with Glu^{190}. When the interface is compared with those of the single mutants, one observes that the network of water molecules is disrupted, where only the two water molecules that interact with Arg^{164} are retained (Supplementary Figure S4B at http://www.bioscirep.org/bsr/032/bsr0320401add.htm). Indeed, a general feature of all of the double mutants as well as the triple mutant is that the interfaces have fewer water molecules, and thus the water-mediated interactions among Arg^{164}, Tyr^{197}, Tyr^{195} and Glu^{124} are disrupted (Supplementary Figure S4). At present, it is not clear whether the loss of the water molecules affects the position of Tyr^{195}.

When Tyr^{197} is replaced with cysteine in the background of V266H [caspase3 (Y197C,V266H)] or E124A,V266H [caspase 3 (E124A,Y197C,V266H)], the enzyme activity returns to levels approximately 10–20-fold lower than the single mutant Y197C or wild-type caspase 3 (Table 1). Both mutants crystallized in the orthorhombic space group I222, with one monomer per asymmetric unit. For the double mutant, Y197C,V266H, the histidine side chain rotates about the φ_2 dihedral angle so that the ε_2-nitrogen atom of each histidine ring faces Arg^{164}, similar to our initial model. The nitrogen atoms in the imidazole ring and those in Arg^{164} and $Arg^{164'}$ are all within 3 Å or less. Although Tyr^{195} does not occupy the same position as in wild-type caspase 3, it is further from Thr^{140}, at 3.4 Å (Figure 3C), and Lys^{137} interacts with Glu^{190} similarly to wild-type caspase 3. Helix 3 is no longer distorted as in the single mutant V266H, and the positions of the short surface β-strands are similar to those of wild-type caspase 3. Similar results are observed for the triple mutant, and for both mutants the electron density shows loop 1 to be well-ordered (Supplementary Figure S8 at http://www.bioscirep.org/bsr/032/bsr0320401add.htm). In the triple mutant, as with monomer B in caspase 3 (E124A,V266H), the electron density supports two conformations for His^{266}. One conformation is similar to that observed in the Y197C,V266H double mutant, where the ε_2-nitrogen atom of each histidine ring faces Arg^{164}. The second conformation is similar to that observed in the E124A,V266H double mutant where the imidazole ring faces the C-terminus of β-strand 8 near Tyr^{195}.

Overall, the structural data for the double and triple variants show that the defects caused by His^{266} are corrected when Tyr^{197}

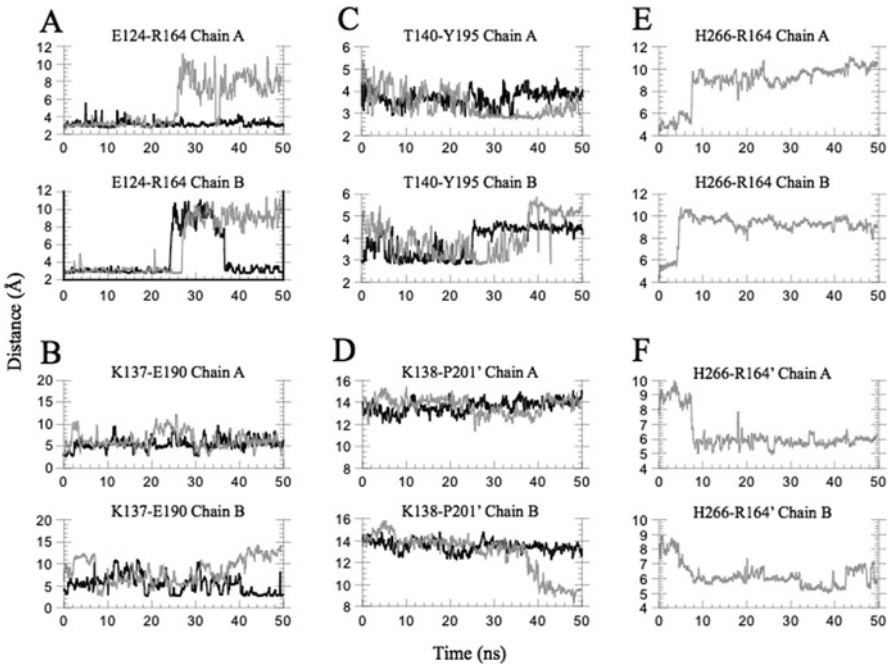

Figure 4 Distances were calculated for atom pairs over the course of the molecular dynamics simulation
Plots indicate distance in Å on the *y*-axis, and simulation time in ns on the *x*-axis. Atom pairs are indicated on each plot. Black refers to wild-type caspase 3, and grey refers to caspase 3 (V266H).

is replaced with cysteine. Interestingly, the electron density supports two conformations for His^{266} when Glu^{124} also is mutated to alanine. In some cases, the position of Tyr^{195} is closer to that in wild-type caspase 3, although it shows much variability, even in mutants that are active. The position of Tyr^{195} in the mutants suggests a larger dynamic range for the Tyr^{195} side chain compared with other residues in the interface, and a survey of caspase 3 crystal structures confirms this conclusion. We examined 23 structures of caspase 3 from the PDB, all with resolution greater than 2.0 Å and in the I222 or $P2_12_12$ space groups (one monomer per asymmetric unit) (Supplementary Table S2 at http://www.bioscirep.org/bsr/032/bsr0320401add.htm), and found little variation in Tyr^{197}, Arg^{164}, Glu^{124}, or Pro^{201}. The position of Tyr^{195}, however, varied such that its distance from Thr^{140} ranged between 3.4 and 4.3 Å (Supplementary Figure S9 at http://www.bioscirep.org/bsr/032/bsr0320401add.htm).

Molecular dynamics simulations

In order to further examine the effects of the mutations, we performed molecular dynamics simulations on the proteins shown in Figure 3(A) for a total of 50 ns. Global structures at the end of the simulations were very similar to those of the crystal structures for all mutants, with RMSDs between 1 and 2 Å (results not shown). For wild-type caspase 3, the results show that for both monomers the N-terminus of loop 2′ is very flexible and does not remain bound near the active site. In addition, L1 also demonstrates a high amount of flexibility (Supplementary Figure S10 at http://www.bioscirep.org/bsr/032/bsr0320401add.htm). With regard to the amino acids described above, at the beginning of the simulation Lys^{137} is 2.7 Å from Glu^{190}, but it quickly moves to an average distance of 5.6 Å and fluctuates between 2.5 and 11.6 Å (with similar values for monomer B), suggesting that the Lys^{137}–Glu^{190} salt bridge is quite dynamic (see Figure 4B). In contrast, the carboxylate moiety of Glu^{124} from monomer A is positioned close to Arg^{164} (2.9 Å) at the beginning of the simulation, and the distance fluctuates only small amounts (2.9–3.3 Å) throughout the simulation. We note, however, that Glu^{124} from monomer B briefly moves out of the interface to a solvent-exposed position (10.3 Å from Arg^{164}) before moving back into the interface (2.8 Å from Arg^{164}) (Figure 4A). Thus, for the time of the simulation, Glu^{124} from monomer A remains in H-bonding distance with Arg^{164}, whereas the interactions are somewhat more transient in monomer B. Finally, the distance between Tyr^{195} and Thr^{140} fluctuates between 2.5 and 5.5 Å over the 50 ns simulation for both monomers (Figure 4C), consistent with our survey of structures described above. The single mutants Y197C and E124A showed similar results as described for wild-type caspase 3 and are not discussed further (results not shown).

In the single mutant, V266H, movements in both monomers occur in a similar manner and so are described as a single event unless otherwise noted. The simulations show that, although the global structure is similar after 50 ns to that of the starting structure (RMSD of 0.89 Å), there are several notable differences in the dimer interface. Within 5 ns of the start of the simulation, the side chain of His^{266} flips to the C-terminal side of β-strand 8,

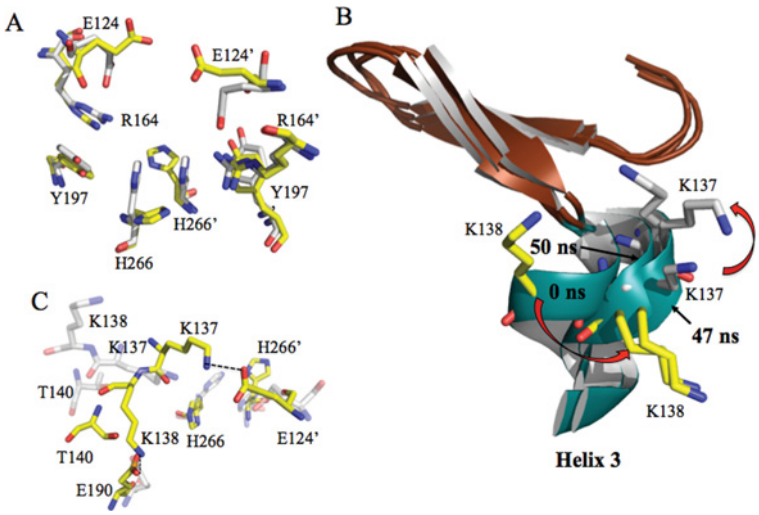

Figure 5 Molecular dynamics simulations show that helix 3 is destabilized in caspase 3 (V266H)
(**A**) Comparison of dimer interface at time zero (X-ray crystal structure) (grey) and 50 ns (yellow). (**B**) Movement of N-terminal region of helix 3. Three time points are shown (0, 47 and 50 ns), and rotations of Lys^{137} and Lys^{138} side chains are indicated by red arrows. (**C**) New interactions observed between Lys^{137} and Glu$^{124'}$ (across interface) and Lys^{138} and Glu^{190} due to rotation of helix 3 (time zero shown in grey, and 50 ns time shown in yellow).

away from Arg^{164}, where it remains throughout the simulation (Figure 5A). In the new position, His^{266} faces Tyr^{195} in a manner similar to that observed in the crystal structures of the double mutant E124A,V266H and the triple mutant. The movement of the His^{266} side chain results in an increase in the distance between Arg^{164} and His^{266} from 4.5 to ~9 Å, although the distance between His^{266} and Arg$^{164'}$ across the interface decreases to between 5 and 6 Å (Figures 4E and 4F, and Supplementary Figures S1E and S1F). When the side chain of His^{266} flips to the C-terminal side of β-strand 8, Tyr^{195} moves closer to helix 3 and fluctuates between distances of 2.9 and 3.9 Å from Thr^{140}. In addition, the side chain of Glu^{124} moves out of the interface to a solvent-exposed position (~8 Å from Arg^{164}) (Figures 4A and 5A). Although the position is similar to that described above for monomer B of wild-type caspase 3, the side chain of Glu^{124} remains in the solvent-exposed position rather than moving back into the interface as observed for wild-type. Later in the simulation, a major rearrangement occurs in helix 3 of monomer B. The N-terminal half of the helix rotates so that the helix is closer to the interface (Figures 4D, 5B and 5C). This movement results in a ~90° rotation of Thr^{140} away from Tyr^{195} as well as movement of Lys^{137} away from Glu^{190}. In this new position, Lys^{137} alternates between H-bonding with the carbonyl moiety of Pro$^{201'}$ and the carboxylate of Glu$^{124'}$, across the interface. In addition, Lys^{138} forms a new H-bond with Glu^{190} (Figure 5C), and the distance between Lys^{138} and Pro$^{201'}$ decreases from 14 Å to less than 10 Å (Figure 4D). Overall, several new interactions occur due to the rotation of helix 3 and the change in Glu^{124} to a solvent-exposed position. In this conformation, the interface is narrower by ~4 Å, and the movement of helix 3 pushes the two short β-strands towards the active site (Figure 5B), resulting in the reduction in volume of the central cavity from ~1750 Å^3 at 30 ns to ~950 Å^3 at 50 ns. For wild-type caspase 3, the volume of the cavity remains constant at ~1900 Å^3 throughout the simulation.

The overall dynamics of each mutant was analysed by comparing the calculated B-factors from each simulation. The dimer interface of wild-type caspase 3 remained largely rigid, with few fluctuations observed (Supplementary Figure S10A). The inactive V266H mutant, however, was much more dynamic over the course of the simulation, particularly with regard to the N-terminus of helix 3, as well as with numerous residues in the dimer interface (Supplementary Figure S10D). This increase in the dynamics of the dimer interface was also observed in the inactive mutants, E124A,V266H and E124A,Y197C (Supplementary Figures S10E and S10F respectively), while the active mutants were closer to wild-type (Supplementary Figures S10B and S10C). The E124A mutation resulted in an increase in motion at the site of the mutation, but this did not necessarily correlate with the loss of activity for the protein, as the E124A single mutant remains active.

In the case of Y197C,V266H, numerous similarities were observed when compared with the results for wild-type caspase 3. For example, Glu^{124} in both monomers remains generally within 3 Å of Arg^{164} (Supplementary Figure S11A at http://www.bioscirep.org/bsr/032/bsr0320401add.htm). In monomer A, the movements of Lys^{137} resemble those of wild-type (Supplementary Figure S11B), and although for monomer B the distance from Glu^{190} fluctuates more than that observed for wild-type, the average distance over the course of the simulation is still somewhat less than for the V266H mutant (7.8 Å compared with 8.5 Å) (Supplementary Figure S11B). In addition, Thr^{140} for both monomers remains within 5 Å of Tyr^{195},

as seen in the simulations for both the wild-type and V266H proteins (Supplementary Figure S11C). In contrast with V266H, where both histidine side chains rotate to face Tyr^{195}, in monomer A of the Y197C,V266H double mutant, His^{266} only momentarily rotates to the C-terminal side of β-strand 8, and within 5 ns moves to a more intermediate distance from Arg^{164} (average of 8.4 Å) when compared with the same interactions in the V266H single mutant (9.4 Å). This position allows for a ring-stacking interaction with Tyr^{195} (Supplementary Figure 12 at http://www.bioscirep.org/bsr/032/bsr0320401add.htm) and is maintained for the majority of the simulation (Supplementary Figures S11E and S11F). Finally, the movements in helix 3 described above for the V266H single mutant are observed in the double mutant, but only transiently at the beginning of the simulation. This change in helix 3 results in a decrease in the distance between the α carbons of residues Lys^{138} and Pro$^{201'}$, from 13 to 10 Å, for less than 2 ns (Supplementary Figure S11D). In the V266H single mutant, this change has occurred by 40 ns, and is maintained for the duration of the simulation. Together, these results are consistent with the observation that the addition of the Y197C mutation was sufficient to restore activity when combined with the V266H mutation because the double mutant more closely resembles the wild-type protein.

In the E124A,Y197C double mutant, which was mostly inactive, numerous differences were observed when compared with wild-type. Although the Y197C,V266H mutant had a transient shift in helix 3, the E124A,Y197C double mutant had much more robust shift in the helix as compared with either V266H or Y197C,V266H. This feature can be observed by a decrease in distance between Lys^{138} and Pro$^{201'}$ from 14 Å to ~10 Å, as well as a longer dwell time in this configuration (Supplementary Figure S11D). Over the course of the simulation, Lys^{137} was an average distance of 10 and 8 Å from Glu^{190} for monomers A and B respectively with very little time spent within hydrogen bonding distance, more closely resembling the results for V266H. In addition, after the first 10 ns of the simulation, Tyr^{195} from monomer A rotated away from Thr^{140} and utilized a different rotamer such that the side chain faced the cavity generated by the mutation of Tyr^{197} to cysteine (Supplementary Figure S12B), increasing the distance from Thr^{140} to ~14 Å (Supplementary Figure S11C). These movements were observed transiently in V266H (monomer B), but the separation was more prevalent for the E124A,Y197C double mutant. Interestingly, helix 3 was observed to move towards the interface, in a manner similar to that observed in the single mutant V266H, as shown by the distance between Lys^{138} and Pro$^{201'}$ (Supplementary Figure S11D). Collectively, the results presented here show that the enzyme can retain activity when either Tyr^{197} or Glu^{124} is mutated, but not both. When mutated together, the E124A,Y197C double mutation results in a dynamic loop between the two surface β-strands, the '124-loop' (Supplementary Figure S10F), destabilization of helix 3 (Supplementary Figure S11D), and an increase in conformational states for Tyr^{195} (Supplementary Figure12B). Importantly, the collective data for this mutant show that there may be several ways to manipulate the allosteric site of the interface to populate the inactive states of caspase 3, apart from mutations at Val^{266}.

Finally, when the three mutations are inserted together, the dynamic range of Y195 is more similar to that of wild-type. In this case, the presence of His^{266} appears to prevent the movement of Tyr^{195} towards the cavity generated by the Tyr^{197} to cysteine mutation (Supplementary Figures S11C and S12B). In addition, helix 3 does not appear to sample the alternate conformation, as shown by the constant distance of Lys^{138} and Pro$^{201'}$ of between 13 and 14 Å (Supplementary Figure S11D). Together, these features may explain the increase in activity when compared with the E124A,Y197C double mutant.

DISCUSSION

In the present study, we examined the consequences of mutating Val^{266} to histidine in the allosteric site of caspase 3. This region of the protein was shown previously to be the site of binding for allosteric inhibitors of caspases 1, 3 and 7 [1,3,7], and a common allosteric mechanism was proposed in which the inhibitors prevent formation of the active conformation by blocking formation of the substrate-binding pocket (loop 3) [1]. A consequence of this mechanism is that Arg^{164} on active site loop 2 remains exposed to solvent. This state has been referred to as the 'off-state' since it resembles the zymogen. The allosteric networks that affect the shift between 'off-state' and 'on-state' have been mutated to decipher the mechanism, so the roles of several key residues are reasonably well understood [3,23]. In the apo-caspase as well as the procaspase, the allosteric site appears to be used in a similar manner in that the IL binds in the site and prevents active site formation by blocking loop movement into the interface [9,10]. Removal of the IL from the allosteric site, either by mutation [8] or binding of substrate is sufficient to allow active site formation. So, a common theme between activating the procaspase versus inhibiting the mature caspase appears to involve stabilizing the active site loops through interactions in the allosteric site or reversing the process respectively.

We showed previously that mutation of Val^{266} to histidine inactivates the protein [2], and we suggested that steric clashes between His^{266} and Tyr^{197} could mimic the effects of the small molecule allosteric inhibitors by preventing insertion of the elbow region of active site loop 3 [11]. The results presented here show that a more accurate representation of the allosteric mechanism includes a consideration of ensembles of active versus inactive conformations rather than discrete states that reflect the positions of the loops. The X-ray crystal structure of caspase 3 (V266H) showed that the histidine side chain was accommodated in the interface, but its presence affected the structure of the active site, resulting in a narrower S1 binding pocket and a disordered loop 1. The structural changes appeared to be propagated through helix 3 on the protein surface and through disruption of H-bonding interactions between Glu^{124} and Arg^{164}. Molecular dynamics simulations of the V266H variant showed that His^{266} moves to the C-terminal side of β-strand 8 and displaces Tyr^{195} towards helix 3. Experimental evidence for this conformation of

His^{266} was observed in the E124A,V266H double mutant as well as the E124A,Y197C,V266H triple mutant. Helix 3 is destabilized such that the N-terminal half of the helix rotates towards the dimer interface, and this conformation is stabilized by new interactions across the interface, particularly between Lys^{137} and Glu$^{124'}$, and Lys^{138} and Glu$^{190'}$. The conformational change does not occur in wild-type caspase 3, at least on the time scale of our experiments. In wild-type caspase 3, Glu^{124} remains inserted into the interface to interact with Arg^{164}, and helix 3 does not sample the extended conformation.

Replacing Glu^{124} with alanine or Tyr^{197} with cysteine individually is not sufficient to shift the population of states to the inactive ensemble, although when combined, the double mutation of E124A,Y197C results in a largely inactive protein with features similar to the single V266H variant. By X-ray crystallography, we observe that helix 3 is distorted as is the active site, and MD simulations show that helix 3 populates the inactive conformation, where it is rotated towards the interface. In addition, when Tyr^{197} is mutated to cysteine, the side chain of Tyr^{195} rotates to fill the cavity generated by the smaller Cys^{197}, but this occurs only if Glu^{124} also is replaced with alanine. A survey of caspase 3 structures shows several positions for the Tyr^{195} side chain, and this was confirmed in our MD simulations of the mutants. Although the structural data for V266H suggest that a H-bond between Tyr^{195} and Thr^{140} stabilizes the C-terminal end of helix 3, the importance of the interaction is not fully revealed in these studies.

In the context of V266H, the active ensemble is repopulated when Tyr^{197} also is replaced with cysteine. In the Y197C,V266H double mutant, Glu^{124} remains inserted in the interface and interacts with Arg^{164}. The presence of His^{266} also likely prevents Tyr^{195} from rotating into the new cavity at Cys^{197}. From the X-ray structural data, these features manifest as an ordered helix 3 and loop 1.

Previous structural data of allosterically inhibited caspases demonstrated large changes in the active site loops, particularly in loop 3, which forms the base of the substrate-binding pocket [1,3,7]. We show here that more subtle conformational changes also inactivate the protein. As we examined structures of proteins with inhibitor bound in the active site, we have compared active and inactive proteins in which the substrate-binding pocket is formed. In all of these structures, Arg^{164} as well as the elbow loop are inserted into the interface. From the structural and MD simulation data for the seven allosteric site mutants, we suggest the following depiction of caspase 3 as part of the inactive ensemble, where one or more of these changes result in inactivation. The side chain of Glu^{124} is exposed to solvent rather than interacting with Arg^{164}. The side chain of Tyr^{195} moves to within H-bonding distance of Thr^{140}, and the N-terminal region of helix 3 rotates towards the interface, allowing interactions across the interface among several charged residues, such as Glu^{124}, Lys^{137}, Lys^{138} and Glu^{190}. As a result of these changes, the volume of the interface is decreased by $\sim$800 Å^3, the S1′ pocket is narrower, and the mobility of loop 1 is increased. The level of activity in each mutant examined here may reflect the extent to which this inactive ensemble is populated. The results also show that one of the changes is generally not sufficient to inactivate the protein, but rather several of the changes must occur together.

It is worth noting that while the '124-loop' is present in all caspases, the specific interactions in the interface are not conserved. In caspase 9 for example, where only one of the two monomers is active, seven residues are inserted in the loop, and the additional amino acids extend across the interface to interact with the extended loop from the second monomer [21]. The longer loops abolish the interface cavity in caspase 9, so presumably the interactions between the two loops stabilize the dimer, possibly at the risk of removing the allosteric control found in other caspases. For caspase 9 and other initiator caspases, the allosteric mechanism may be coupled to dimerization, as natural protein inhibitors bind to this site to form heterocomplexes [24,25]. Although the equivalent to Arg^{164} is conserved in caspase 1 (Arg^{286} in caspase 1 numbering), the equivalent of Glu^{124} is not utilized (Glu^{241} in caspase 1) because a glutamate on β-strand 8 forms a salt bridge with Arg^{286} [1,3].

As all caspases contain the catalytic histidine–cysteine dyad and because they require an aspartyl moiety in the P1 position, it has proven difficult to design tight-binding and specific caspase inhibitors. In contrast, small molecule inhibitors to the allosteric site of the interface show more promise because the interface differs for the caspase subfamilies. Current allosteric inhibitors of caspases 1, 3 and 7 stabilize the 'off-state' of the enzyme [1,3,7,23]. The results presented here suggest that in addition to the better-characterized 'off-state', the inactive ensemble also contains states in which the substrate-binding loop is formed. The design of allosteric modulators may take into account these more subtle changes in the allosteric site to shift the population to the inactive ensemble, such as stabilizing helix 3 in the extended conformation, for example. One would predict that such inhibitors would show high specificity since the allosteric site differs among caspases and may be of value for caspase-related therapeutics.

AUTHOR CONTRIBUTION

Jad Walters prepared the proteins, conducted enzyme activity measurements and solved structures of the proteins. Josh Schipper performed and analysed the molecular dynamics simulations. Paul Swartz solved the structures by X-ray crystallography and analysed the molecular dynamics simulations. Carla Mattos and Clay Clark designed the experiments and wrote the paper.

FUNDING

This work was supported by the National Institutes of Health [grant number GM065970 (to A.C.C.)]. Use of the Advanced Photon Source was supported by the U.S. Department of Energy, Office of Science, Office of Basic Energy Sciences, under contract number W-31-109-ENG-38.

REFERENCES

1 Scheer, J. M., Romanowski, M. J. and Wells, J. A. (2006) A common allosteric site and mechanism in caspases. Proc. Natl. Acad. Sci. U.S.A. **103**, 7595–7600
2 Pop, C., Feeney, B., Tripathy, A. and Clark, A. C. (2003) Mutations in the procaspase-3 dimer interface affect the activity of the zymogen. Biochemistry **42**, 12311–12320
3 Datta, D., Scheer, J. M., Romanowski, M. J. and Wells, J. A. (2008) An allosteric circuit in caspase-1. J. Mol. Biol. **381**, 1157–1167
4 Wolan, D. W., Zorn, J. A., Gray, D. C. and Wells, J. A. (2009) Small-molecule activators of a proenzyme. Science **326**, 853–858
5 Boatright, K. M. and Salvesen, G. S. (2003) Mechanisms of caspase activation. Curr. Opin. Cell Biol. **15**, 725–731
6 Schipper, J. L., MacKenzie, S. H., Sharma, A. and Clark, A. C. (2011) A bifunctional allosteric site in the dimer interface of procaspase-3. Biophys. Chem. **159**, 100–109
7 Hardy, J. A., Lam, J., Nguyen, J. T., O'Brien, T. and Wells, J. A. (2004) Discovery of an allosteric site in the caspases. Proc. Natl. Acad. Sci. U.S.A. **101**, 12461–12466
8 Walters, J., Pop, C., Scott, F. L., Drag, M., Swartz, P., Mattos, C., Salvesen, G. S. and Clark, A. C. (2009) A consitutively active and uninhibitable caspase-3 zymogen efficiently induces apoptosis. Biochem. J. **424**, 335–345
9 Chai, J., Wu, Q., Shiozaki, E., Srinivasula, S. M., Alnemri, E. S. and Shi, Y. (2001) Crystal structure of a procaspase-7 zymogen: mechanisms of activation and substrate binding. Cell **107**, 399–407
10 Riedl, S. J., Fuentes-Prior, P., Renatus, M., Kairies, N., Krapp, S., Huber, R., Salvesen, G. S. and Bode, W. (2001) Structural basis for the activation of human procaspase-7. Proc. Natl. Acad. Sci. U.S.A. **98**, 14790–14795
11 MacKenzie, S. H. and Clark, A. C. (2008) Targeting cell death in tumors by activating caspases. Curr. Cancer Drug Targets **8**, 98–109
12 Bose, K., Pop, C., Feeney, B. and Clark, A. C. (2003) An uncleavable procaspase-3 mutant has a lower catalytic efficiency but an active site similar to that of mature caspase-3. Biochemistry **42**, 12298–12310
13 Feeney, B., Pop, C., Swartz, P., Mattos, C. and Clark, A. C. (2006) Role of loop bundle hydrogen bonds in the maturation and activity of (pro)caspase-3. Biochemistry **45**, 13249–13263
14 Walters, J., Swartz, P., Mattos, C. and Clark, A. C. (2011) Thermodynamic, enzymatic and structural effects of removing a salt bridge at the base of loop 4 in (pro)caspase-3. Arch. Biochem. Biophys. **508**, 31–38
15 Stennicke, H. R. and Salvesen, G. S. (1999) Caspases: preparation and characterization. Methods **17**, 313–319
16 Feeney, B., Pop, C., Tripathy, A. and Clark, A. C. (2004) Ionic interactions near loop L4 are important for maintaining the active site environment and the dimer stability of (pro)caspase-3. Biochem. J. **384**, 515–525
17 Hess, B., Kutzner, C., van der Spoel, D. and Lindahl, E. (2008) GROMACS 4: Algorithms for highly efficient, load-balanced, and scalable molecular simulation. J. Chem. Theory Comp. **4**, 435–447
18 Wang, J., Cieplak, P. and Kollman, P. A. (2000) How well does a restrained electrostatic potential (RESP) model perform in calculating conformational energies of organic and biological molecules? J. Comp. Chem. **21**, 1049–1074
19 Jorgensen, W. L., Chandrasekhar, J., Madura, J. D., Impey, R. W. and Klein, M. L. (1983) Comparison of simple potential functions for simulating liquid water. J. Chem. Phys. **79**, 926–935
20 Essmann, U., Perera, L., Berkowitz, M. L., Darden, T., Lee, H. and Pedersen, L. G. (1995) A smooth particle mesh Ewald method. J. Chem. Phys. **103**, 8577–8593
21 Renatus, M., Stennicke, H. R., Scott, F. L., Liddington, R. C. and Salvesen, G. S. (2001) Dimer formation drives the activation of the cell death protease caspase 9. Proc. Natl. Acad. Sci. U.S.A. **98**, 14250–14255
22 Witkowski, W. A. and Hardy, J. A. (2009) L2′ loop is critical for caspase-7 active site formation. Protein Sci. **18**, 1459–1468
23 Hardy, J. A. and Wells, J. A. (2009) Dissecting an allosteric switch in caspase-7 using chemical and mutational probes. J. Biol. Chem. **284**, 26063–26069
24 Shiozaki, E. N., Chai, J., Rigotti, D. J., Riedl, S. J., Li, P., Srinivasula, S. M., Alnemri, E. S., Fairman, R. and Shi, Y. (2003) Mechanism of XIAP-mediated inhibition of caspase-9. Mol. Cell **11**, 519–527
25 Yu, J. W., Jeffrey, P. D. and Shi, Y. (2009) Mechanism of procaspase-8 activation by c-flipl. Proc. Natl. Acad. Sci. **106**, 8169–8174

Received 4 May 2012/16 May 2012; accepted 18 May 2012
Published as Immediate Publication 18 May 2012, doi 10.1042/BSR20120037

Biosci. Rep. (2012) / **32** / 401–411 (Printed in Great Britain) / doi 10.1042/BSR20120037

online data

Original Paper

SUPPLEMENTARY ONLINE DATA

Allosteric modulation of caspase 3 through mutagenesis

Jad WALTERS*, Joshua L. SCHIPPER*, Paul SWARTZ*, Carla MATTOS*[1] and A. Clay CLARK*†[2]

*Department of Molecular and Structural Biochemistry, North Carolina State University, Raleigh, NC 27695, U.S.A., and †Center for Comparative Medicine and Translational Research, North Carolina State University, Raleigh, NC 27695, U.S.A.

MATERIALS AND METHODS

Site-directed mutagenesis of caspase 3

The single mutants V266H, Y197C and E124A were made in the background of wild-type caspase 3 using site-directed mutagenesis and plasmid pHC332 as a template [1]. All mutations were confirmed by sequencing both DNA strands, and the mutated bases are shown in bold. For V266H, primers 1 and 2 were used: 5′- CAGATTCCATGTATT**CA**-TAGCATGCTCACAAAAGAACTC-3′ and 5′-GAGTTCTTT-TGTGAGCATGCTA**TG**AATACA-TGGAATCTG-3′, respectively. For Y197C, primers 3 and 4 were used: 5′-GGCCGAC-TTCTT-GTATGCAT**GC**A**GT**AC**T**GCACCTGG-3′ and 5′-CCAGGTGCAGTACTGCATGCATACAAG-AAGTCGGCC-3′ respectively. For E124A, primers 5 and 6 were used: 5′-CTG-AGCCATGGTGAAG**CC**GGCATAATTTTTGGAAC-3′ and 5′-GTTCCAAAAATTATGCCGGCTTCACCAT-GGCTCAG-3′ respectively. Primers 1, 2, 3 and 4 introduced a unique SphI site. Primers 5 and 6 introduced a unique NaeI site (underlined). The resulting plasmids (in pET21b) are referred to as pHC33203, pHC33226 and pHC33247 for the V266H, Y197C and E124A single mutants respectively.

The double mutants Y197C,V266H and E124A,V266H mutations were made in the background of V266H using plasmid pHC33203 as a template. For Y197C,V266H, primers 7 and 8 were used: 5′-GGCCGACTTCTTGTATGCAT**GC**A**GT**A**T**G-CACCTGG-3′ and 5′-CCAGGTGCAGTA-CTGCATGCATA-CAAGAAGTCGGCC-3′ respectively. For E124A,V266H, primers 9 and 10 were used: 5′-CTGAGCCATGGTGAA-G**CC**GGCATAATTTTTGGAAC-3′ and 5′-GTTCCA-AAAAT-TATGCCGGCTTCACCATGG CTCAG -3′ respectively. Primers 7 and 8 introduced a SphI site, while primers 9 and 10 introduced a NaeI site (underlined). The resulting plasmids are referred to as pHC33227 and pHC33271 for the Y197C,V266H and E124A,V266H double mutants respectively.

The double mutant E124A,Y197C was made in the background of Y197C using plasmid pHC33226 as a template. For E124A,Y197C, primers 11 and 12 were used: 5′-CTG-AGCCATGGTGAAG**CC**GGCATAATTTTTGGAAC-3′ and –GTTCCAAAAATTATGC-CGGCTTCACCATGGCTCAG-3′ respectively. Primers 11 and 12 introduce a unique NaeI site. The resulting plasmid for E124A,Y197C is referred to as pHC33270.

The triple mutant, E124A,Y197C,V266H was made in the background of Y197C,V266H using plasmid pHC33227 as a template and primers 13 and 14: 5′-CT-GAGCCATGGTGAAG**CC**GG**C**ATAATTTTTGGAAC-3′ and 5′-GTTCCAA-AAATTATGCCGGCTTCACCATGGCTCAG-3′. Primers 13 and 14 introduce a unique NaeI site. The resulting plasmid for E124A,Y197C,V266H is referred to as pHC33272.

[1] Present address: Department of Chemistry and Chemical Biology, Northeastern University, 102 Hurtig Hall, 360 Huntington Ave, Boston, MA 02115, U.S.A.
[2] To whom correspondence should be addressed (email clay_clark@ncsu.edu).

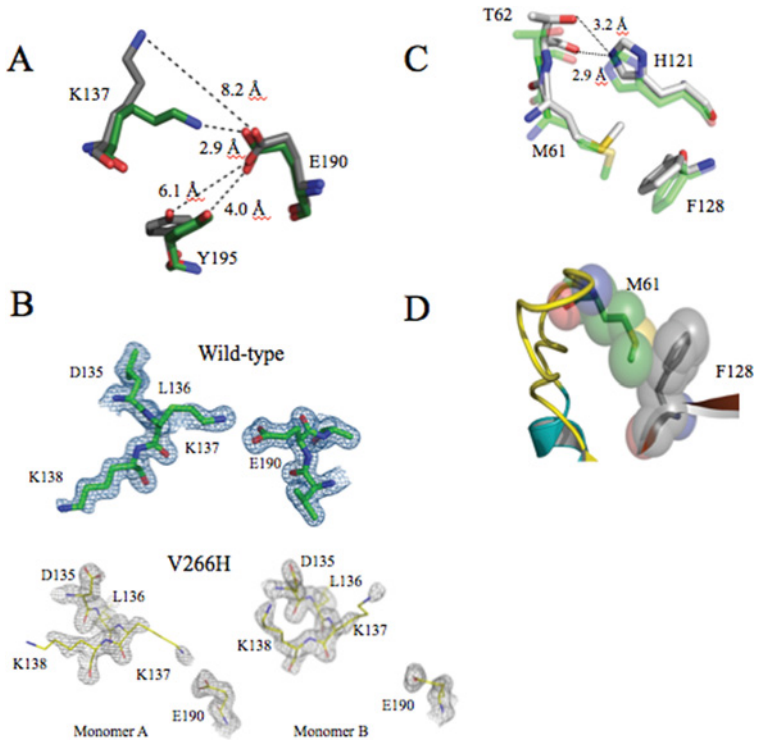

Figure S1 **Changes in caspase 3 resulting from V266 to histidine mutation**
(**A**) Interactions among Lys[137], Glu[190] and Tyr[195] showing increases in distances for V266H variant (grey) versus wild-type (green). (**B**) Electron density maps for Lys[137] and Glu[190] for wild-type (upper panel) or V266H variant (lower panel). (**C**) Comparison of active site for wild-type (green) versus V266H variant (grey) demonstrating different rotamer for Met[61] and increased H-bonding distance for the catalytic residue His[121]. (**D**) Steric clashes between Phe[128] and Met[61] result in the different rotamer observed in (**C**).

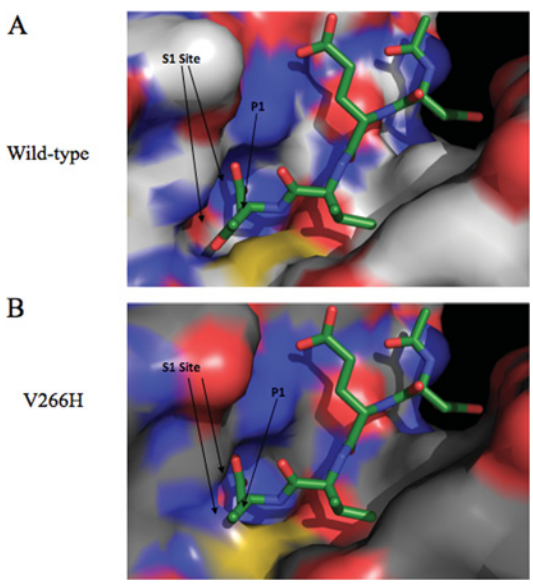

Figure S2 The S1 and S1′ sites are wider in wild-type caspase 3
(**A**) Compared with the V266H variant (**B**).

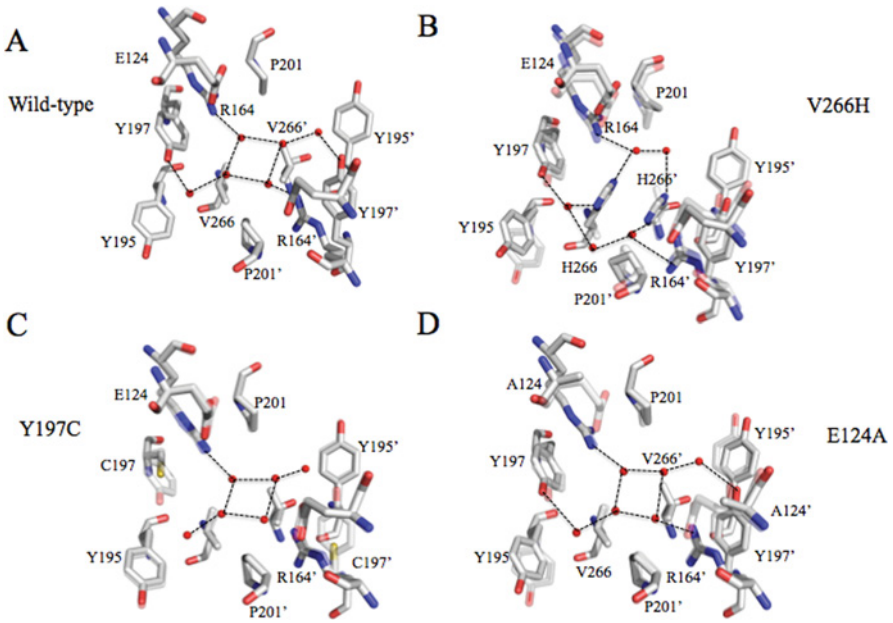

Figure S3 **Comparison of H-bonding and water molecules in the dimer interface of wild-type caspase 3 (A) and single mutants V266H (B), Y197C (C) or E124A (D)**
(**A**–**D**) Red spheres indicate water molecules, and the prime (′) indicates amino acids from the second monomer. For (**B**–**D**), Wild-type caspase 3 is shown as partially transparent.

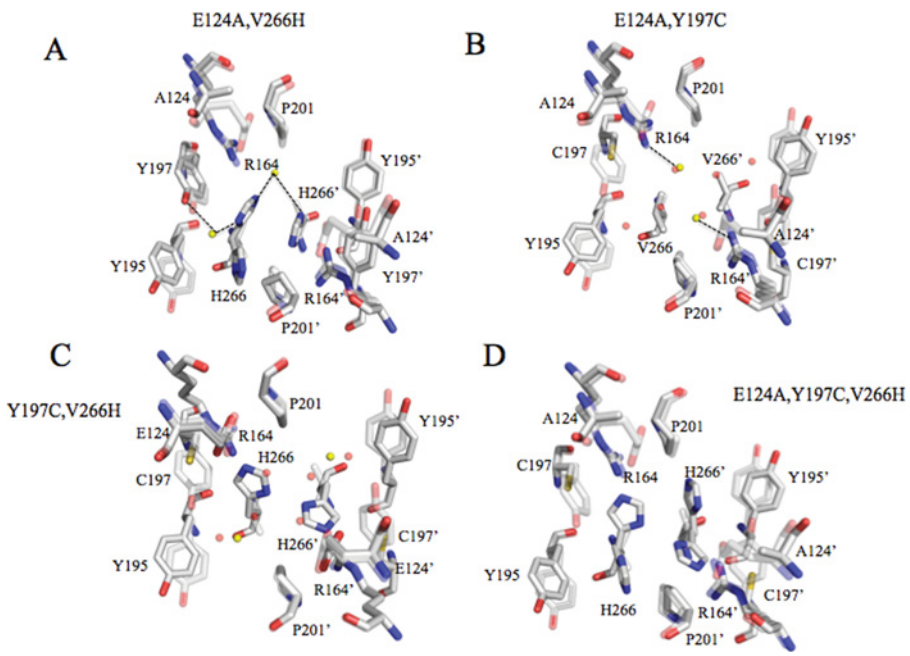

Figure S4 **Comparison of H-bonding and water molecules in the dimer interface of wild-type caspase 3 and double mutants E124A,V266H (A) E124A,Y197C (B), Y197C,V266H (C) and triple mutant E124A,Y197C,V266H (D)**
(**A**–**D**) Red spheres indicate water molecules in wild-type caspase 3 and yellow spheres indicate water molecules in the mutant. The prime (′) indicates amino acids from the second monomer, and wild-type caspase 3 is shown as partially transparent.

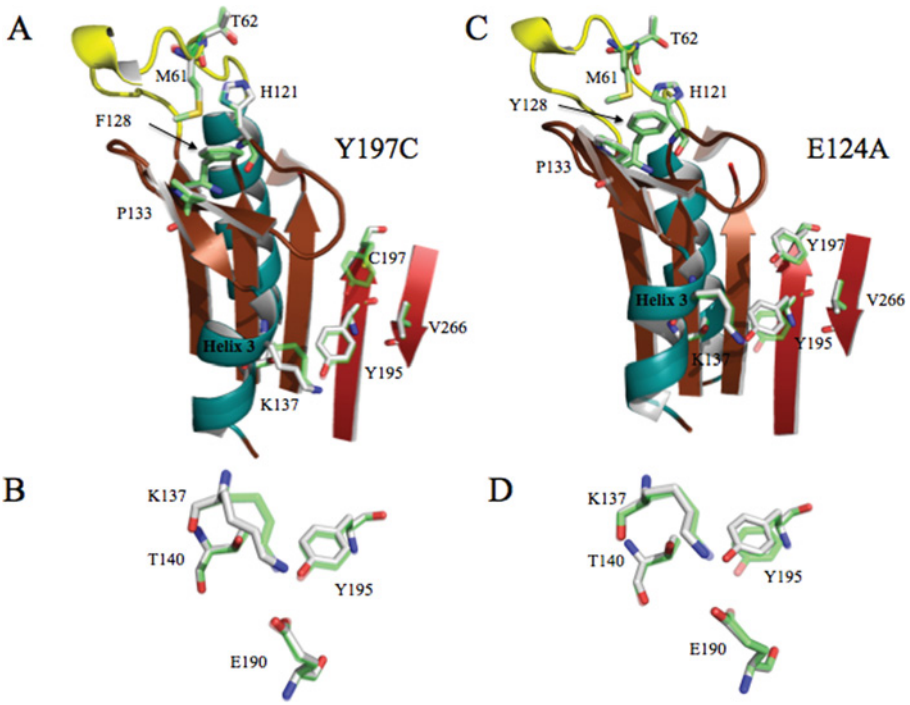

Figure S5 **Comparison of single mutants Y197C (A, B) or E124A (C, D) with wild-type caspase 3**
(**A**–**D**) Wild-type caspase 3 is shown as partially transparent and amino acid side chains are coloured green. Amino acid side-chains for the mutants are coloured grey.

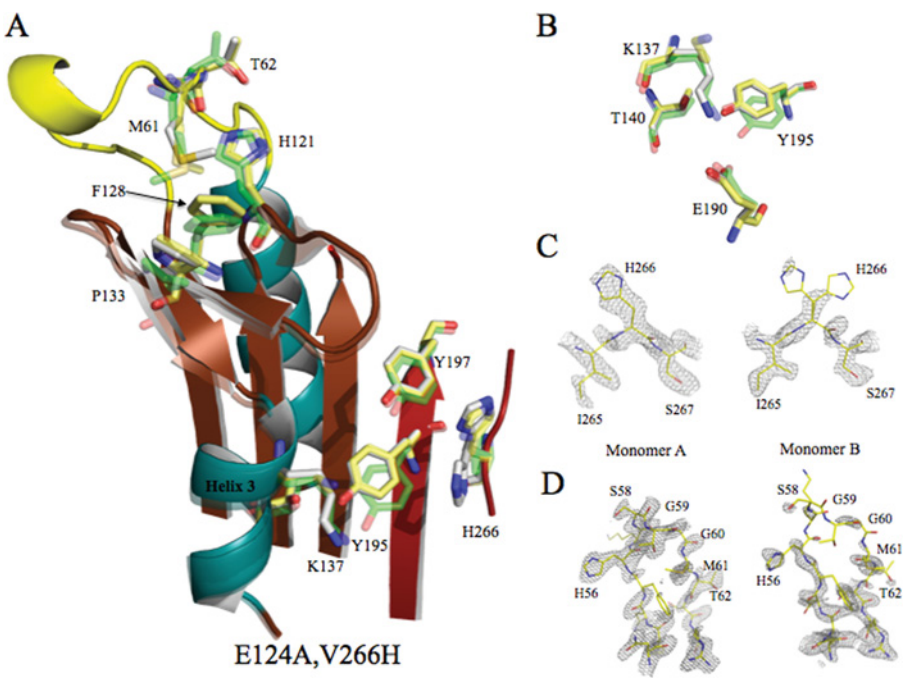

Figure S6 **Comparison of the double mutant E124A,V266H (grey) with V266H (yellow) and wild-type (green) caspase 3**
(**A**) Changes in helix 3 and active site regions due to the mutations. (**B**) Comparison of interactions among Lys^{137}, Thr^{140}, Glu^{190} and Tyr^{195}. (**C**) Electron density maps of His^{266} in monomer A (left panel) or monomer B (right panel) demonstrating evidence for two conformations of His^{266} in monomer B. (**D**) Electron density maps of L1 of monomer A (left panel) or monomer **B** (right panel) demonstrating disorder in L1 of monomer B. For (**C**, **D**), the mesh is drawn at $\sigma = 2.0$.

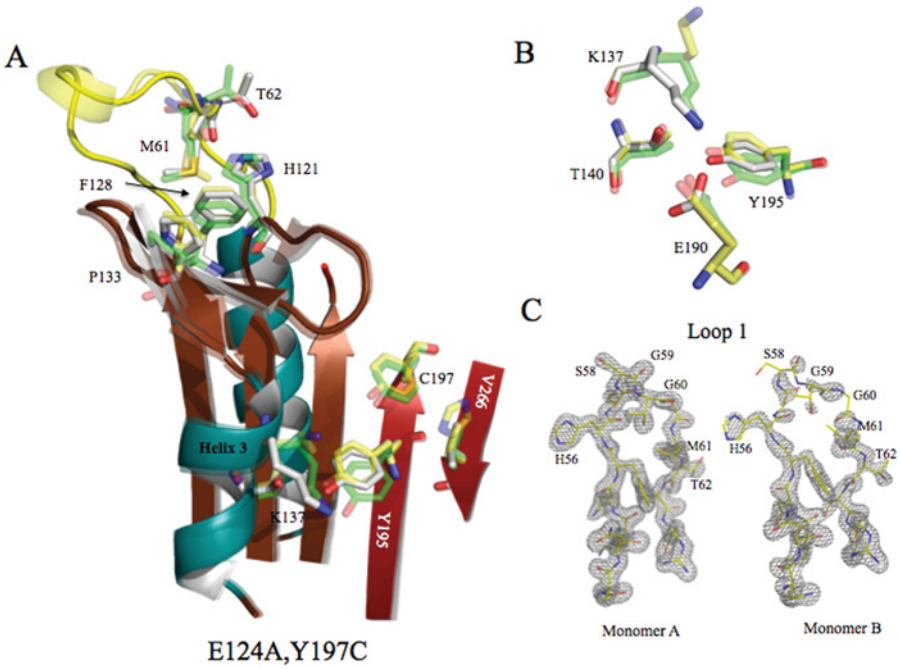

Figure S7 **Comparison of the double mutant E124A,Y197C (grey) with V266H (yellow) and wild-type (green) caspase 3**
(**A**) Changes in helix 3 and active site regions due to the mutations. (**B**) Comparison of interactions among Lys^{137}, Thr^{140}, Glu^{190} and Tyr^{195}. (**C**) Electron density maps of L1 of monomer A (left panel) or monomer B (right panel) demonstrating disorder in L1 of monomer B. For (**C**) the mesh is drawn at $\sigma = 2.0$.

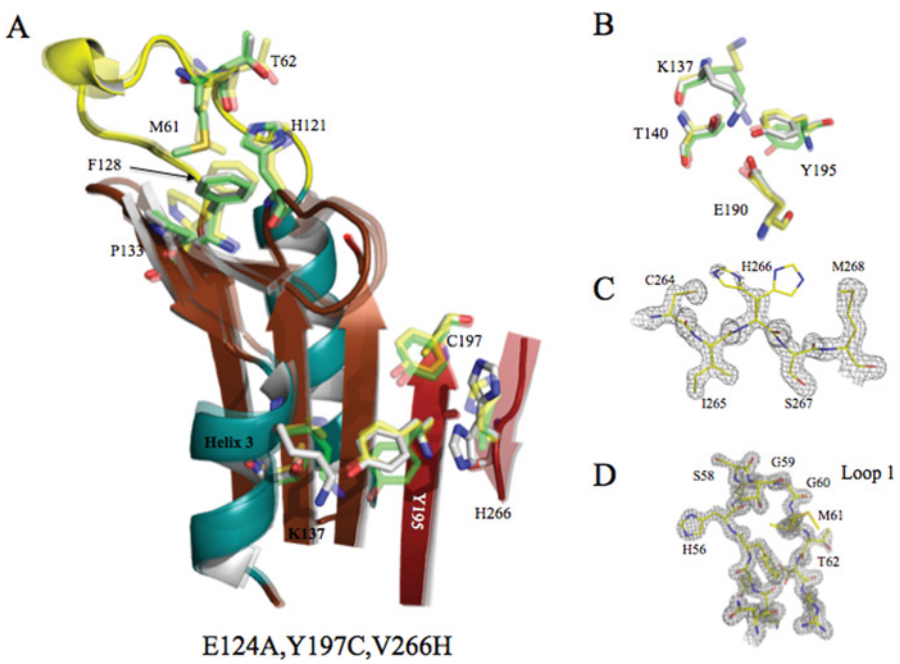

Figure S8 **Comparison of the triple mutant E124A,Y197C,V266H (grey) with V266H (yellow) and wild-type (green) caspase 3**
(**A**) Changes in helix 3 and active site regions due to the mutations. (**B**) Comparison of interactions among Lys^{137}, Thr^{140}, Glu^{190} and Tyr^{195}. (**C**) Electron density map of His^{266} demonstrating evidence for two conformations of His^{266}. (**D**) Electron density map of L1 demonstrating order in L1. For (**C**, **D**), the mesh is drawn at $\sigma = 1.5$.

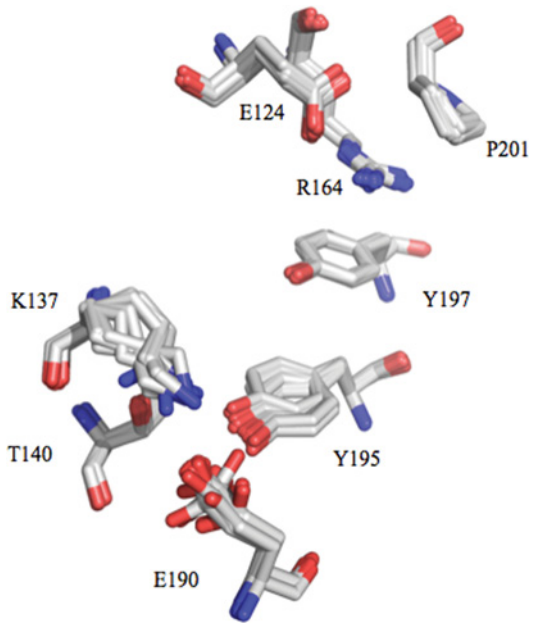

Figure S9 Comparison of indicated amino acid side chains in 23 structures of caspase 3 from the protein data bank, as shown in Table S2

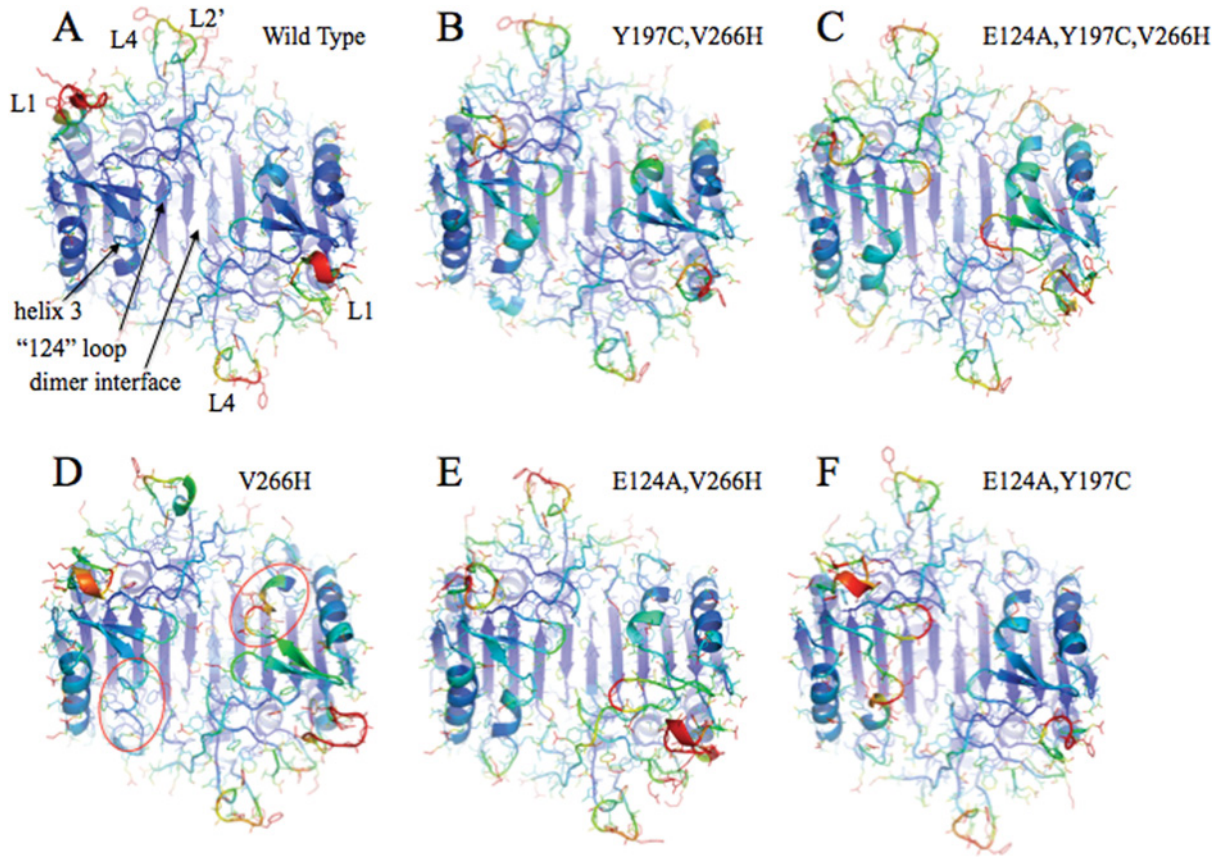

Figure S10 **Structures representing the final frame of the simulation (50 ns) with b-factors indicated by colour**
A blue to red spectrum indicates low to high b-factors respectively, with values greater than 100 set as red. Active site loops 1, 4 and 2′ and regions discussed in the text (dimer interface, '124' loop, helix 3) are indicated in (**A**). Helix 3 is indicated by the red ovals for the V266H variant (**D**). Enzymatically active mutants are shown in the top row (**A**–**C**), and inactive mutants are shown in the bottom row (**D**–**F**).

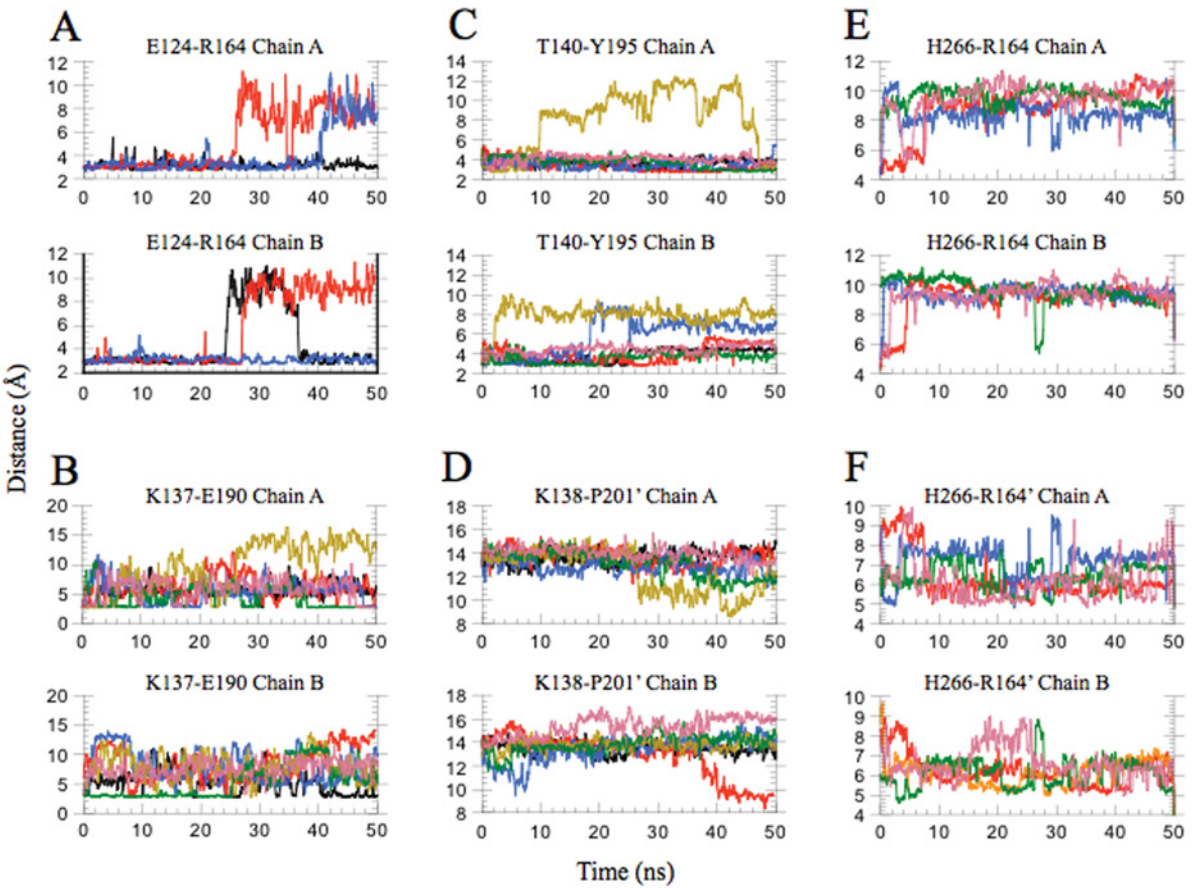

Figure S11 **Distances were calculated for atom pairs over the course of the molecular dynamics simulation**
Plots indicate distance in Å on the *y*-axis, and simulation time in ns on the *x*-axis. Atom pairs are indicated on each plot. The following colour scheme is used for each protein: wild-type (black), V266H (red), Y197C,V266H (blue), E124A,Y197C (olive), E124A,V266H (green) and E124A,Y197C,V266H (purple).

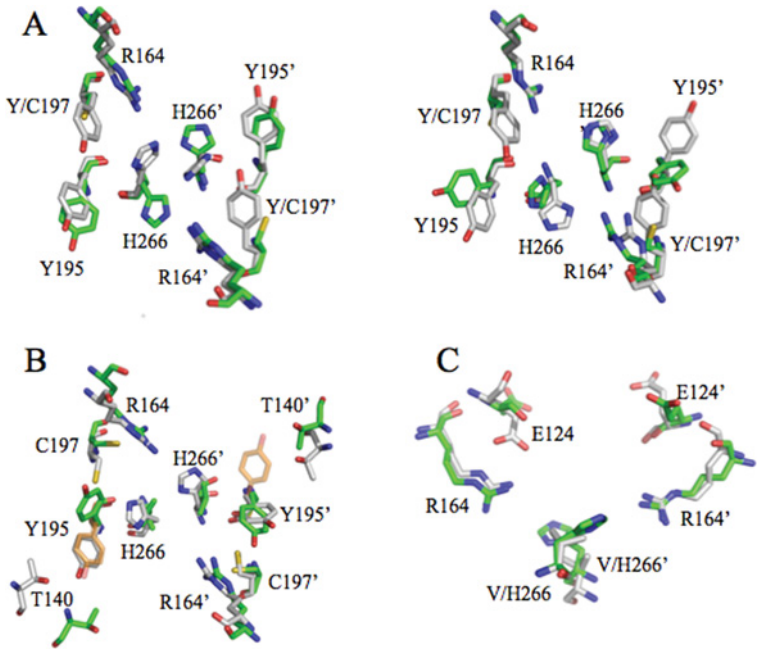

Figure S12 **Comparison of conformations of key residues in the dimer interface from molecular dynamics simulations** (**A**) Movement of His^{266} for the V266H (grey) and Y197C,V266H (green) variants at 2 ns (left) and 50 ns (right). (**B**) In monomer B of Y197C,V266H (grey), at 30 ns Tyr^{195} moves from the native orientation (wild-type conformation shown in orange) and points towards the cavity introduced by Cys^{197}. This movement occurs in both monomers of the E124A,Y197C variant (green). (**C**) At 30 ns, Glu^{124} in monomer B of wild-type caspase 3 (grey) transiently moves to a solvent-exposed position. In the V266H variant (green), the same movement for Glu^{124} is observed in both monomers, and the side-chain remains in the solvent-exposed position for the duration of the simulation. For (**A**–**C**), monomer B is indicated by the prime (′) notation.

Table S1 Summary of data collection and refinement statistics

Parameter	Wild-type*	V266H	Y197C	E124A	Y197C, V266H	E124A, V266H	E124A, Y197C	E124A, Y197C,V266H
Space group	I222	C2	I222	I222	I222	C2	C2	I222
Unit cell								
a (Å)	68.73	109.91	69.33	69.02	68.55	109.36	109.82	68.89
b (Å)	84.40	96.77	84.49	84.75	84.60	96.73	96.78	85.52
c (Å)	96.35	69.78	95.92	96.26	96.48	69.21	69.18	96.34
α (°)	90	90	90	90	90	90	90	90
β (°)	90	127.19	90	90	90	127.11	127.39	90
γ (°)	90	90	90	90	90	90	90	90
Temperature (K)	100	100	100	100	100	100	100	100
Resolution (Å)	1.40	1.70	1.64	1.78	1.72	1.86	1.68	1.69
Number of reflections	54 279	54 485	36 196	25 638	33 032	33 894	64 820	31 715
Completeness (%)	97.9	84.7	93.2	93.5	97.7	63.7	97.1	98.5
Redundancy	5.8	3.5	4.8	6.4	4.8	1.7	3.5	4.6
Average I/σ	46.2 (1.34)	36.7 (11.6)	15.1 (5.9)	20.2 (1.99)	28.4 (11.9)	40.4 (14.6)	49.2 (16.7)	20.0 (6.3)
R_{work} (%)	19.6	19.8	18.0	23.8	16.2	16.0	19.6	16.0
R_{free} (%)	20.7	23.3	19.9	28.1	18.5	21.0	23.0	19.2
R_{merge} (%)†	5.9	6.5	13.2	17.3	11.1	6.6	5.1	6.6
RMSD for bond lengths (Å)	0.005	0.007	0.007	0.007	0.007	0.007	0.007	0.007
RMSD for bond angles (°)	1.30	1.15	1.14	1.10	1.19	1.06	1.15	1.12
No. of protein atoms	1974	3905	2060	1996	2086	3848	3824	1989
No. of water molecules	290	386	263	239	207	369	401	261

*PDB code 2J30.

†$R_{merge} = \Sigma_h \Sigma_i |I(h,i) - I(h)| / \Sigma_h \Sigma_i I(h,i)$, where $I(h,i)$ values are symmetry-related intensities and $I(h)$ is the mean intensity of the reflection with unique index h. $R_{work} = \Sigma_h |F_{obs}| - |F_{calc}| / \Sigma |F_{obs}|$,where F_{obs} and F_{calc} are observed and calculated structure factors respectively. $R_{free} = \Sigma_T |F_{obs}| - |F_{calc}| / \Sigma_T |F_{obs}|$,where T is a test dataset of 10% of the total reflections randomly chosen and set aside prior to refinement.

Table S2 Structure files used to compare the position of Tyr^{195}

PDB code	Resolution (Å)	Space group
1QX3	1.9	$P2_12_12$
1NME	1.6	I222
2CJY	1.67	I222
2CJX	1.7	I222
2DKO	1.06	I222
2H5I	1.69	I222
2C2M	1.94	I222
2C2K	1.87	I222
2C1E	1.77	I222
2J30	1.4	I222
2J31	1.5	I222
2J32	1.3	I222
2J33	2.0	I222
2CDR	1.7	I222
2CNO	1.95	I222
2CNN	1.7	I222
2CNL	1.67	I222
2CNK	1.75	I222
3ITN	1.63	I222
3KJF	2.0	$P2_12_12$
3PDO	2.0	I222
3PD1	1.62	I222
3PCX	1.5	I222

REFERENCE

1 Pop, C., Chen, Y.-R., Smith, B., Bose, K., Bobay, B., Tripathy, A., Franzen, S. and Clark, A. C. (2001) Removal of the pro-domain does not affect the conformation of the procaspase-3 dimer. Biochemistry **40**, 14224–14235

Received 4 May 2012/16 May 2012; accepted 18 May 2012
Published as Immediate Publication 18 May 2012, doi 10.1042/BSR20120037

Biosci. Rep. (2012) / **32** / 401–411 (Printed in Great Britain) / doi 10.1042/BSR20120037

online data

Original Paper

SUPPLEMENTARY ONLINE DATA

Allosteric modulation of caspase 3 through mutagenesis

Jad WALTERS*, Joshua L. SCHIPPER*, Paul SWARTZ*, Carla MATTOS*[1] and A. Clay CLARK*†[2]

*Department of Molecular and Structural Biochemistry, North Carolina State University, Raleigh, NC 27695, U.S.A., and †Center for Comparative Medicine and Translational Research, North Carolina State University, Raleigh, NC 27695, U.S.A.

MATERIALS AND METHODS

Site-directed mutagenesis of caspase 3

The single mutants V266H, Y197C and E124A were made in the background of wild-type caspase 3 using site-directed mutagenesis and plasmid pHC332 as a template [1]. All mutations were confirmed by sequencing both DNA strands, and the mutated bases are shown in bold. For V266H, primers 1 and 2 were used: 5′- CAGATTCCATGTATT**CA**-TAGCATGCTCACAAAAGAACTC-3′ and 5′-GAGTTCTTT-TGTGAGCATGCTA**TG**AATACA-TGGAATCTG-3′, respectively. For Y197C, primers 3 and 4 were used: 5′-GGCCGAC-TTCTT-GTATGCAT**GC**A**GT**AC**T**GCACCTGG-3′ and 5′-CCAGGTGCAGTACTGCATGCATACAAG-AAGTCGGCC-3′ respectively. For E124A, primers 5 and 6 were used: 5′-CTG-AGCCATGGTGAAG**CC**GGCATAATTTTTGGAAC-3′ and 5′-GTTCCAAAAATTATGCCGGCTTCACCAT-GGCTCAG-3′ respectively. Primers 1, 2, 3 and 4 introduced a unique SphI site. Primers 5 and 6 introduced a unique NaeI site (underlined). The resulting plasmids (in pET21b) are referred to as pHC33203, pHC33226 and pHC33247 for the V266H, Y197C and E124A single mutants respectively.

The double mutants Y197C,V266H and E124A,V266H mutations were made in the background of V266H using plasmid pHC33203 as a template. For Y197C,V266H, primers 7 and 8 were used: 5′-GGCCGACTTCTTGTATGCAT**GC**A**GT**A**T**G-CACCTGG-3′ and 5′-CCAGGTGCAGTA-CTGCATGCATA-CAAGAAGTCGGCC-3′ respectively. For E124A,V266H, primers 9 and 10 were used: 5′-CTGAGCCATGGTGAA-G**CC**GGCATAATTTTTGGAAC-3′ and 5′-GTTCCA-AAAAT-TATGCCGGCTTCACCATGG CTCAG -3′ respectively. Primers 7 and 8 introduced a SphI site, while primers 9 and 10 introduced a NaeI site (underlined). The resulting plasmids are referred to as pHC33227 and pHC33271 for the Y197C,V266H and E124A,V266H double mutants respectively.

The double mutant E124A,Y197C was made in the background of Y197C using plasmid pHC33226 as a template. For E124A,Y197C, primers 11 and 12 were used: 5′-CTG-AGCCATGGTGAAG**CC**GGCATAATTTTTGGAAC-3′ and –GTTCCAAAAATTATGC-CGGCTTCACCATGGCTCAG-3′ respectively. Primers 11 and 12 introduce a unique NaeI site. The resulting plasmid for E124A,Y197C is referred to as pHC33270.

The triple mutant, E124A,Y197C,V266H was made in the background of Y197C,V266H using plasmid pHC33227 as a template and primers 13 and 14: 5′-CT-GAGCCATGGTGAAG**CC**GG**C**ATAATTTTTGGAAC-3′ and 5′-GTTCCAA-AAATTATGCCGGCTTCACCATGGCTCAG-3′. Primers 13 and 14 introduce a unique NaeI site. The resulting plasmid for E124A,Y197C,V266H is referred to as pHC33272.

[1] Present address: Department of Chemistry and Chemical Biology, Northeastern University, 102 Hurtig Hall, 360 Huntington Ave, Boston, MA 02115, U.S.A.
[2] To whom correspondence should be addressed (email clay_clark@ncsu.edu).

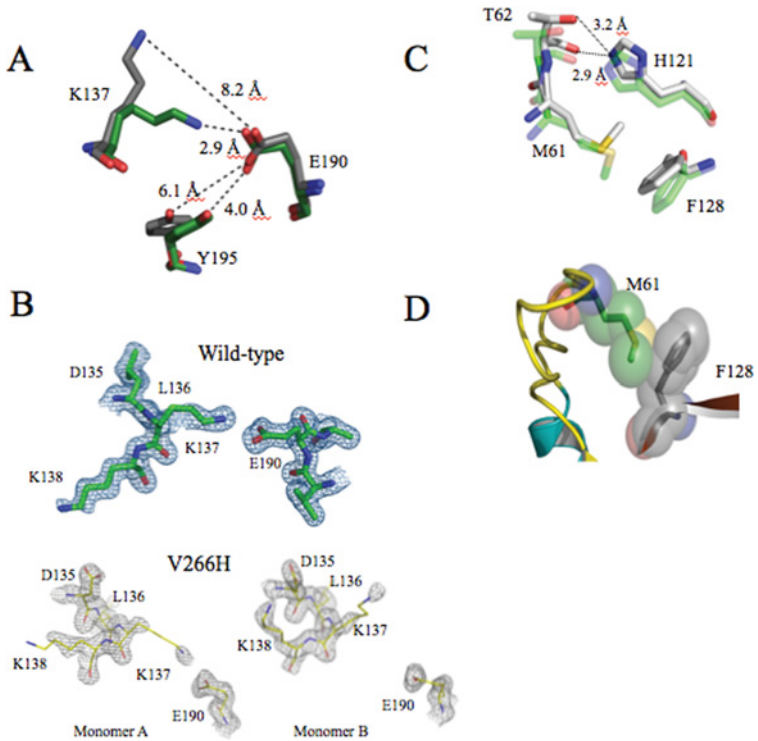

Figure S1 **Changes in caspase 3 resulting from V266 to histidine mutation**
(**A**) Interactions among Lys[137], Glu[190] and Tyr[195] showing increases in distances for V266H variant (grey) versus wild-type (green). (**B**) Electron density maps for Lys[137] and Glu[190] for wild-type (upper panel) or V266H variant (lower panel). (**C**) Comparison of active site for wild-type (green) versus V266H variant (grey) demonstrating different rotamer for Met[61] and increased H-bonding distance for the catalytic residue His[121]. (**D**) Steric clashes between Phe[128] and Met[61] result in the different rotamer observed in (**C**).

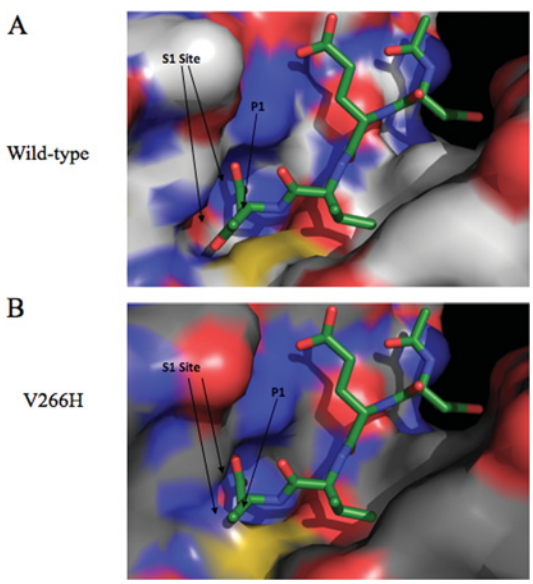

Figure S2 The S1 and S1′ sites are wider in wild-type caspase 3
(**A**) Compared with the V266H variant (**B**).

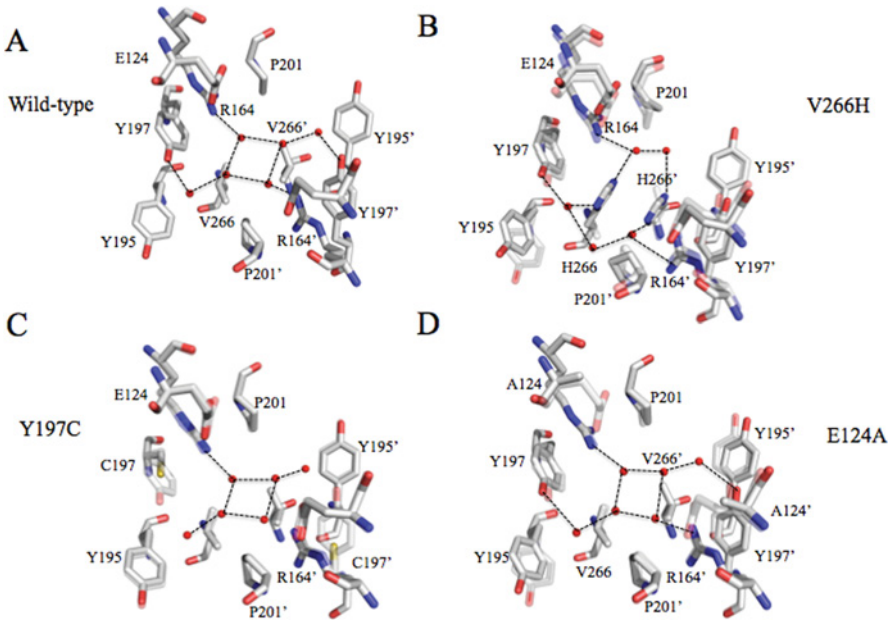

Figure S3 **Comparison of H-bonding and water molecules in the dimer interface of wild-type caspase 3 (A) and single mutants V266H (B), Y197C (C) or E124A (D)**
(**A**–**D**) Red spheres indicate water molecules, and the prime (′) indicates amino acids from the second monomer. For (**B**–**D**), Wild-type caspase 3 is shown as partially transparent.

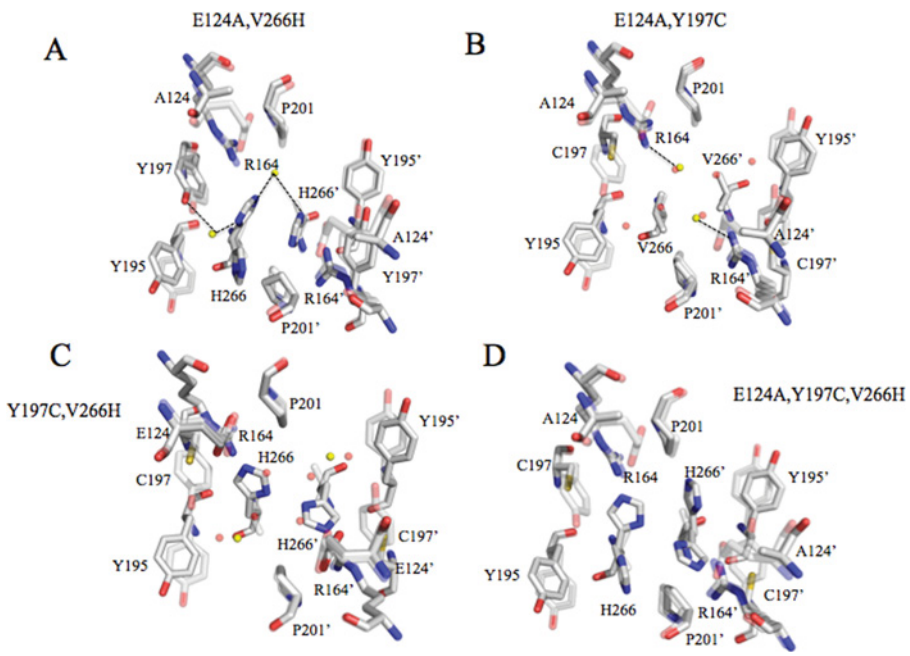

Figure S4 **Comparison of H-bonding and water molecules in the dimer interface of wild-type caspase 3 and double mutants E124A,V266H (A) E124A,Y197C (B), Y197C,V266H (C) and triple mutant E124A,Y197C,V266H (D)**
(**A**–**D**) Red spheres indicate water molecules in wild-type caspase 3 and yellow spheres indicate water molecules in the mutant. The prime (′) indicates amino acids from the second monomer, and wild-type caspase 3 is shown as partially transparent.

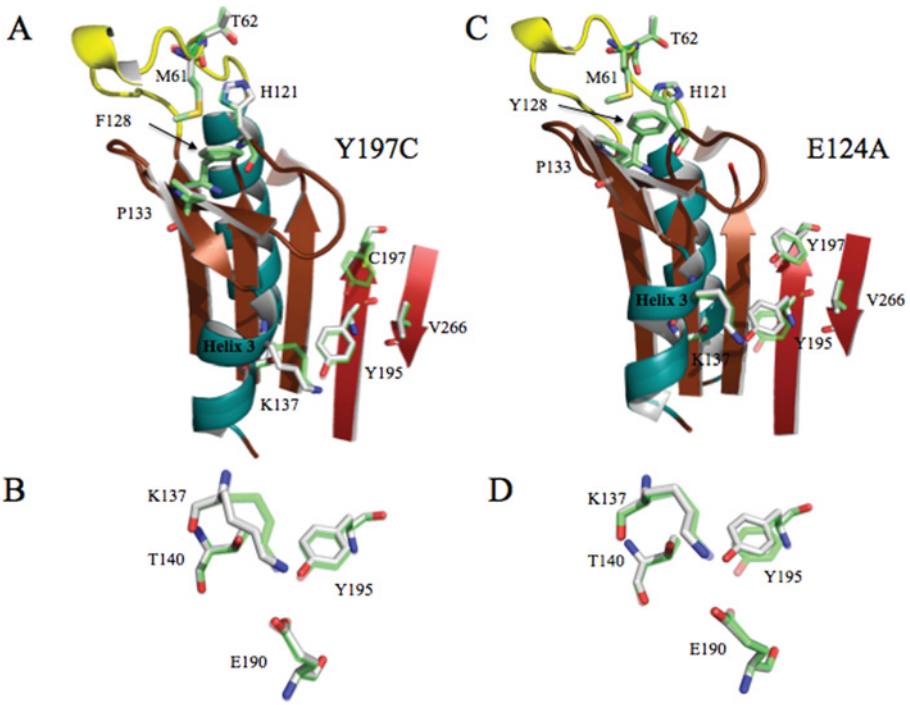

Figure S5 **Comparison of single mutants Y197C (A, B) or E124A (C, D) with wild-type caspase 3**
(**A**–**D**) Wild-type caspase 3 is shown as partially transparent and amino acid side chains are coloured green. Amino acid side-chains for the mutants are coloured grey.

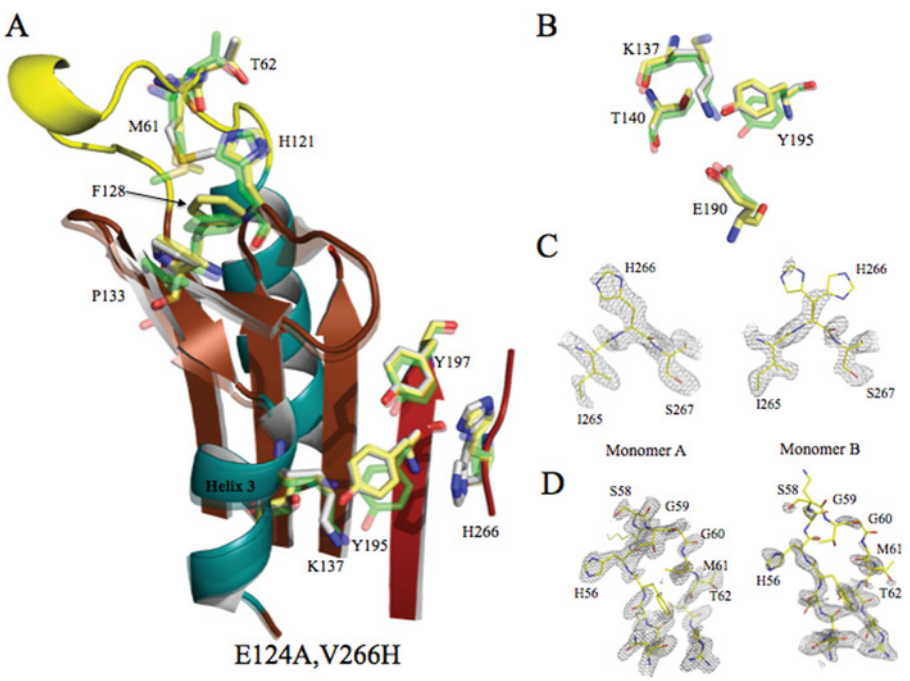

Figure S6 **Comparison of the double mutant E124A,V266H (grey) with V266H (yellow) and wild-type (green) caspase 3**
(**A**) Changes in helix 3 and active site regions due to the mutations. (**B**) Comparison of interactions among Lys^{137}, Thr^{140}, Glu^{190} and Tyr^{195}. (**C**) Electron density maps of His^{266} in monomer A (left panel) or monomer B (right panel) demonstrating evidence for two conformations of His^{266} in monomer B. (**D**) Electron density maps of L1 of monomer A (left panel) or monomer **B** (right panel) demonstrating disorder in L1 of monomer B. For (**C**, **D**), the mesh is drawn at $\sigma = 2.0$.

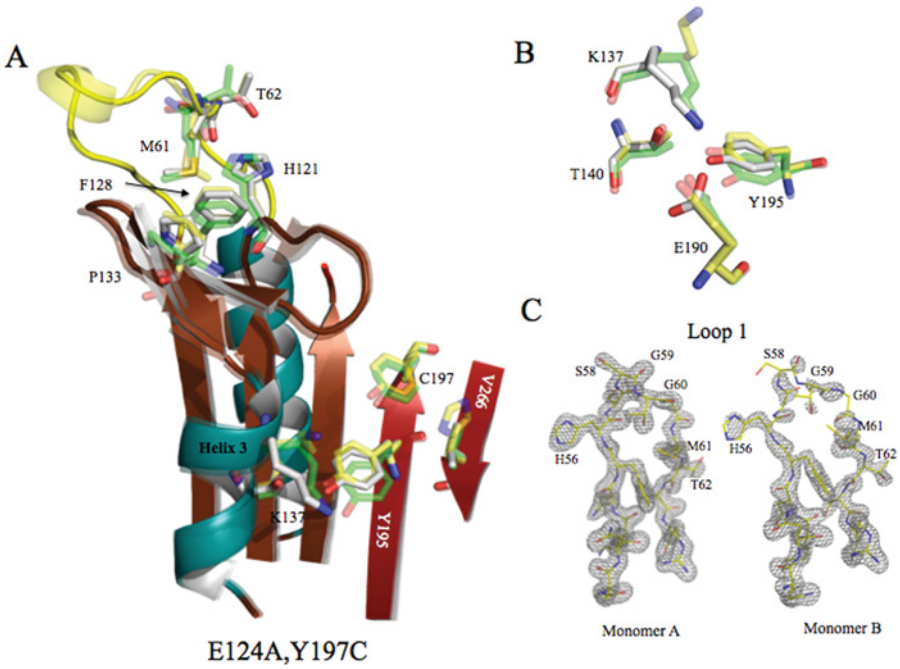

Figure S7 **Comparison of the double mutant E124A,Y197C (grey) with V266H (yellow) and wild-type (green) caspase 3**
(**A**) Changes in helix 3 and active site regions due to the mutations. (**B**) Comparison of interactions among Lys^{137}, Thr^{140}, Glu^{190} and Tyr^{195}. (**C**) Electron density maps of L1 of monomer A (left panel) or monomer B (right panel) demonstrating disorder in L1 of monomer B. For (**C**) the mesh is drawn at $\sigma = 2.0$.

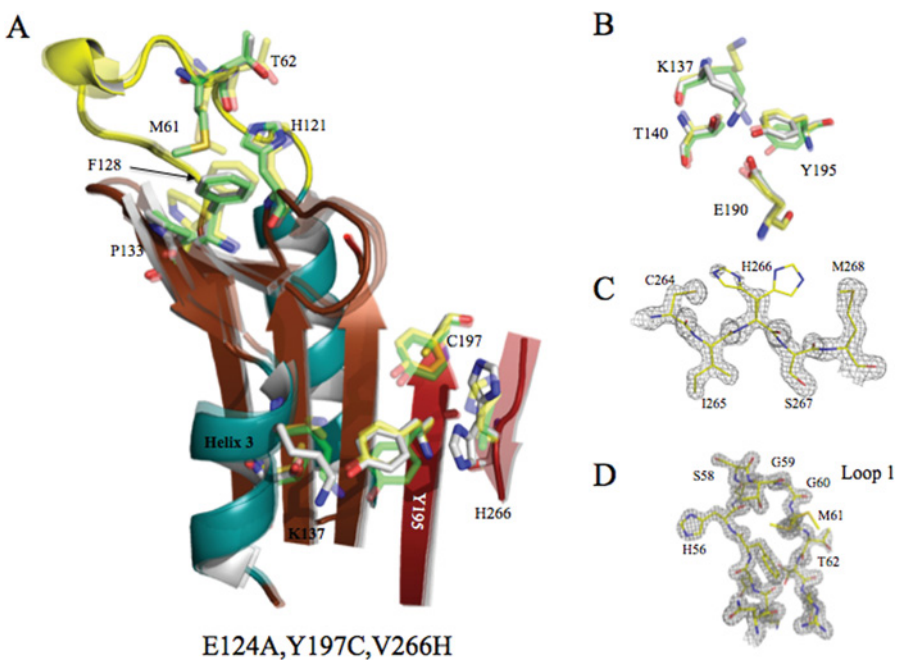

Figure S8 **Comparison of the triple mutant E124A,Y197C,V266H (grey) with V266H (yellow) and wild-type (green) caspase 3**
(**A**) Changes in helix 3 and active site regions due to the mutations. (**B**) Comparison of interactions among Lys^{137}, Thr^{140}, Glu^{190} and Tyr^{195}. (**C**) Electron density map of His^{266} demonstrating evidence for two conformations of His^{266}. (**D**) Electron density map of L1 demonstrating order in L1. For (**C**, **D**), the mesh is drawn at $\sigma = 1.5$.

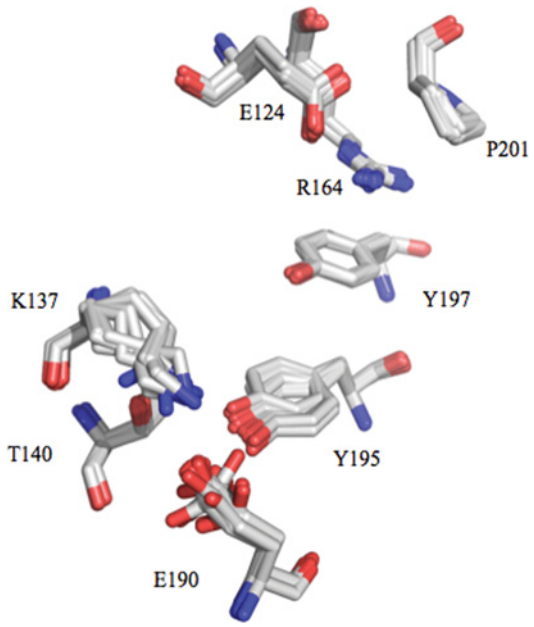

Figure S9 Comparison of indicated amino acid side chains in 23 structures of caspase 3 from the protein data bank, as shown in Table S2

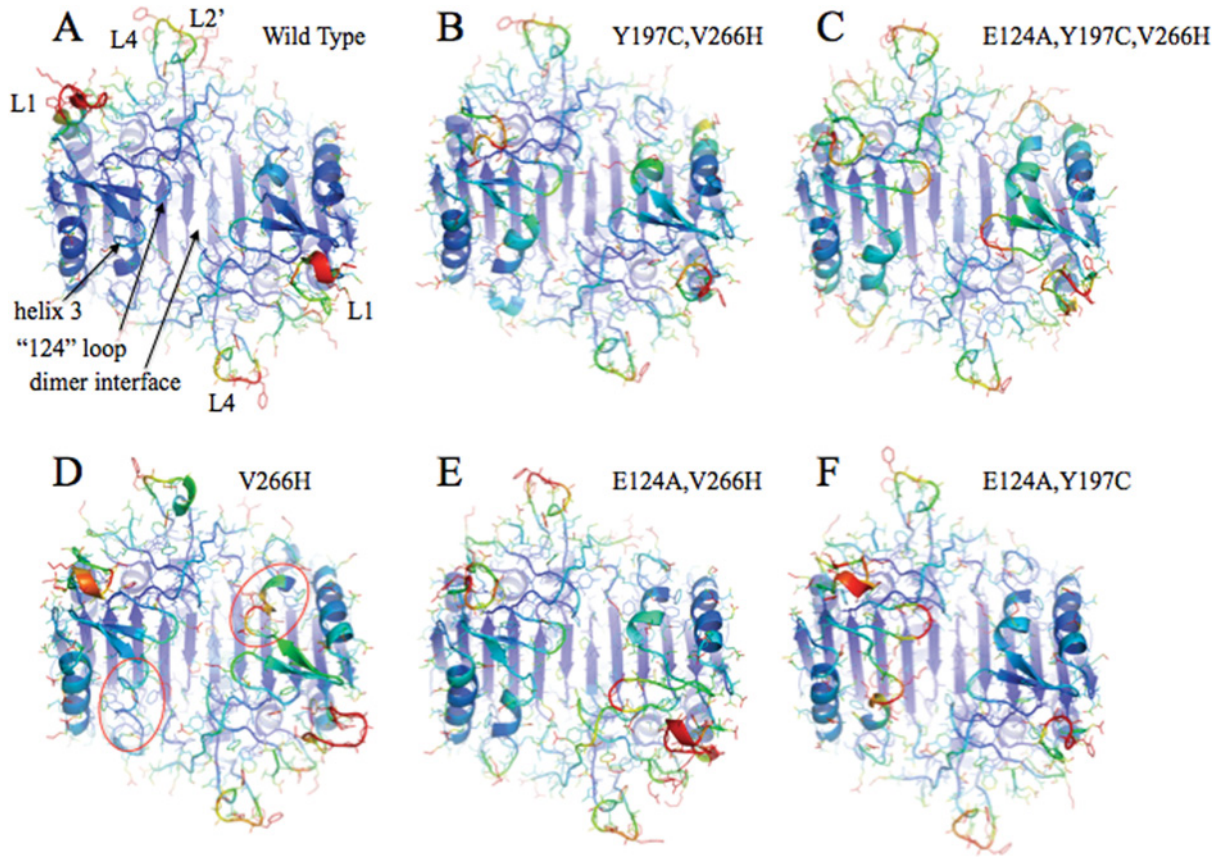

Figure S10 **Structures representing the final frame of the simulation (50 ns) with b-factors indicated by colour**
A blue to red spectrum indicates low to high b-factors respectively, with values greater than 100 set as red. Active site loops 1, 4 and 2′ and regions discussed in the text (dimer interface, '124' loop, helix 3) are indicated in (**A**). Helix 3 is indicated by the red ovals for the V266H variant (**D**). Enzymatically active mutants are shown in the top row (**A**–**C**), and inactive mutants are shown in the bottom row (**D**–**F**).

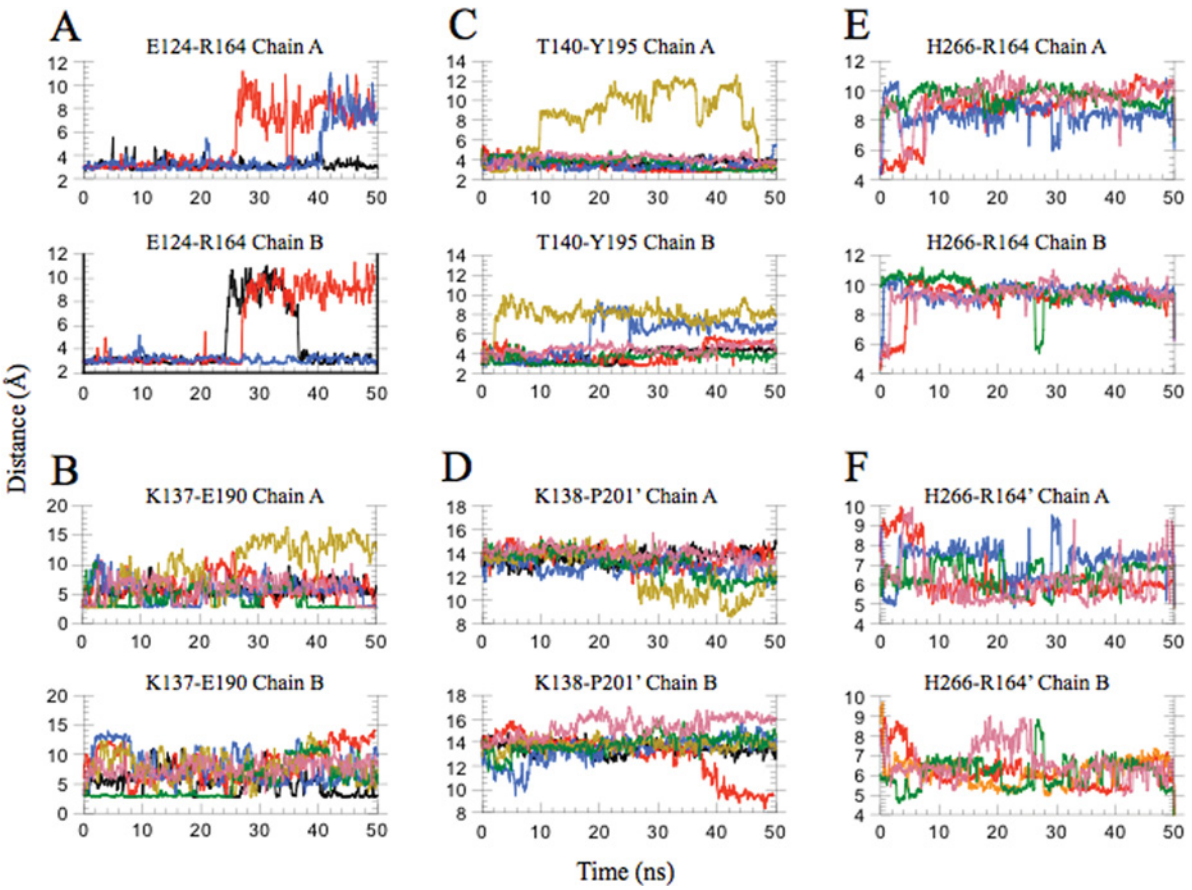

Figure S11 **Distances were calculated for atom pairs over the course of the molecular dynamics simulation**
Plots indicate distance in Å on the *y*-axis, and simulation time in ns on the *x*-axis. Atom pairs are indicated on each plot. The following colour scheme is used for each protein: wild-type (black), V266H (red), Y197C,V266H (blue), E124A,Y197C (olive), E124A,V266H (green) and E124A,Y197C,V266H (purple).

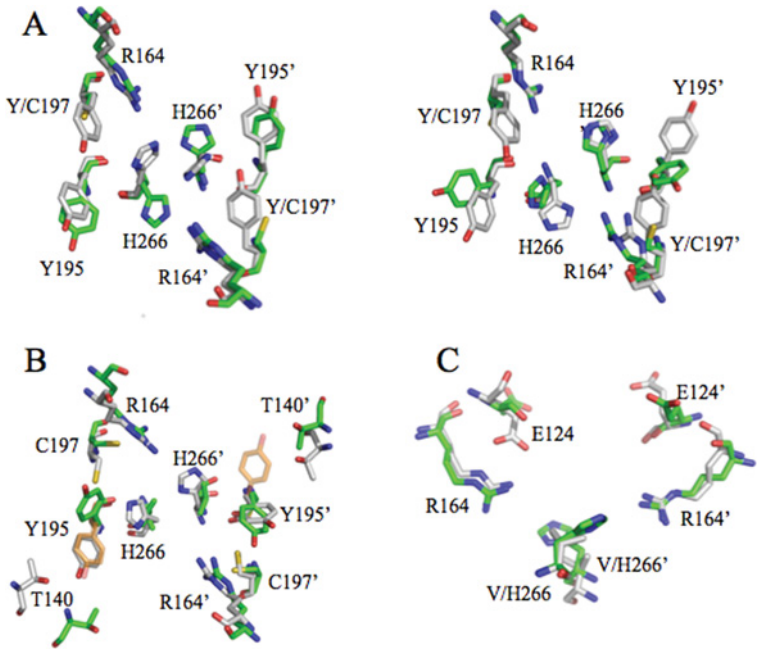

Figure S12 **Comparison of conformations of key residues in the dimer interface from molecular dynamics simulations** (**A**) Movement of His^{266} for the V266H (grey) and Y197C,V266H (green) variants at 2 ns (left) and 50 ns (right). (**B**) In monomer B of Y197C,V266H (grey), at 30 ns Tyr^{195} moves from the native orientation (wild-type conformation shown in orange) and points towards the cavity introduced by Cys^{197}. This movement occurs in both monomers of the E124A,Y197C variant (green). (**C**) At 30 ns, Glu^{124} in monomer B of wild-type caspase 3 (grey) transiently moves to a solvent-exposed position. In the V266H variant (green), the same movement for Glu^{124} is observed in both monomers, and the side-chain remains in the solvent-exposed position for the duration of the simulation. For (**A**–**C**), monomer B is indicated by the prime (′) notation.

Table S1 Summary of data collection and refinement statistics

Parameter	Wild-type*	V266H	Y197C	E124A	Y197C, V266H	E124A, V266H	E124A, Y197C	E124A, Y197C,V266H
Space group	I222	C2	I222	I222	I222	C2	C2	I222
Unit cell								
a (Å)	68.73	109.91	69.33	69.02	68.55	109.36	109.82	68.89
b (Å)	84.40	96.77	84.49	84.75	84.60	96.73	96.78	85.52
c (Å)	96.35	69.78	95.92	96.26	96.48	69.21	69.18	96.34
α (°)	90	90	90	90	90	90	90	90
β (°)	90	127.19	90	90	90	127.11	127.39	90
γ (°)	90	90	90	90	90	90	90	90
Temperature (K)	100	100	100	100	100	100	100	100
Resolution (Å)	1.40	1.70	1.64	1.78	1.72	1.86	1.68	1.69
Number of reflections	54 279	54 485	36 196	25 638	33 032	33 894	64 820	31 715
Completeness (%)	97.9	84.7	93.2	93.5	97.7	63.7	97.1	98.5
Redundancy	5.8	3.5	4.8	6.4	4.8	1.7	3.5	4.6
Average I/σ	46.2 (1.34)	36.7 (11.6)	15.1 (5.9)	20.2 (1.99)	28.4 (11.9)	40.4 (14.6)	49.2 (16.7)	20.0 (6.3)
R_{work} (%)	19.6	19.8	18.0	23.8	16.2	16.0	19.6	16.0
R_{free} (%)	20.7	23.3	19.9	28.1	18.5	21.0	23.0	19.2
R_{merge} (%)†	5.9	6.5	13.2	17.3	11.1	6.6	5.1	6.6
RMSD for bond lengths (Å)	0.005	0.007	0.007	0.007	0.007	0.007	0.007	0.007
RMSD for bond angles (°)	1.30	1.15	1.14	1.10	1.19	1.06	1.15	1.12
No. of protein atoms	1974	3905	2060	1996	2086	3848	3824	1989
No. of water molecules	290	386	263	239	207	369	401	261

*PDB code 2J30.

†$R_{merge} = \Sigma_h \Sigma_i |I(h,i) - I(h)| / \Sigma_h \Sigma_i I(h,i)$, where $I(h,i)$ values are symmetry-related intensities and $I(h)$ is the mean intensity of the reflection with unique index h. $R_{work} = \Sigma_h |F_{obs}| - |F_{calc}| / \Sigma |F_{obs}|$,where F_{obs} and F_{calc} are observed and calculated structure factors respectively. $R_{free} = \Sigma_T |F_{obs}| - |F_{calc}| / \Sigma_T |F_{obs}|$,where T is a test dataset of 10% of the total reflections randomly chosen and set aside prior to refinement.

Table S2 Structure files used to compare the position of Tyr^{195}

PDB code	Resolution (Å)	Space group
1QX3	1.9	$P2_12_12$
1NME	1.6	I222
2CJY	1.67	I222
2CJX	1.7	I222
2DKO	1.06	I222
2H5I	1.69	I222
2C2M	1.94	I222
2C2K	1.87	I222
2C1E	1.77	I222
2J30	1.4	I222
2J31	1.5	I222
2J32	1.3	I222
2J33	2.0	I222
2CDR	1.7	I222
2CNO	1.95	I222
2CNN	1.7	I222
2CNL	1.67	I222
2CNK	1.75	I222
3ITN	1.63	I222
3KJF	2.0	$P2_12_12$
3PDO	2.0	I222
3PD1	1.62	I222
3PCX	1.5	I222

REFERENCE

1 Pop, C., Chen, Y.-R., Smith, B., Bose, K., Bobay, B., Tripathy, A., Franzen, S. and Clark, A. C. (2001) Removal of the pro-domain does not affect the conformation of the procaspase-3 dimer. Biochemistry **40**, 14224–14235

Received 4 May 2012/16 May 2012; accepted 18 May 2012
Published as Immediate Publication 18 May 2012, doi 10.1042/BSR20120037